Pergamon

*Int. J. Solids Structures* Vol. 32, No. 1, pp. 27–62, 1995

0020–7683/95 $9.50 + .00

0020–7683(94)00097–2

# MULTIPLE SCALE ANALYSIS OF HETEROGENEOUS ELASTIC STRUCTURES USING HOMOGENIZATION THEORY AND VORONOI CELL FINITE ELEMENT METHOD

SOMNATH GHOSH, KYUNGHOON LEE and SURESH MOORTHY
Department of Engineering Mechanics, The Ohio State University, Columbus, OH 43210, U.S.A.

(*Received* 8 *February* 1994; *in revised form* 26 *May* 1994)

**Abstract**—This paper deals with the development of a multiple scale finite element method by combining the asymptotic homogenization theory with Voronoi cell finite element method (VCFEM) for microstructural modeling. The Voronoi cell finite element model originates from Dirichlet tessellation of a representative material element or a base cell in the microstructure. Homogenized material coefficients for a global displacement finite element model are generated by VCFEM analysis using periodic boundary conditions on the base cell. Following the macroscopic analysis, the local VCFEM analysis is implemented to depict the true evolution of microstructural stresses and strains. Various numerical examples are executed for validating the effectiveness of VCFEM macro–micro modeling of elastic materials. The effect of size, shape, orientation and distribution of heterogeneities on the local and global response are examined.

## 1. INTRODUCTION

The last three decades have seen tremendous developments in science and technology for heterogeneous materials. Notable among these materials are alloy systems containing precipitates and pores, and polymer, ceramic or metal–matrix composite materials containing a dispersion of fibers, whiskers or particulates in the matrix. In reinforced composites, stiff and strong second phase inclusions of glass, graphite, boron or aluminum oxide, etc. are added to epoxy, steel, titanium or aluminum matrices to enhance strength, thermal expansion coefficient and wear resistance of structures. The degree of mechanical and thermal property enhancements depends on the size, shape and properties of the second phase inclusions as well as on their spatial distribution within the matrix. These functionally superior materials have found increasing utilization in the aerospace, automotive and ordnance industries for replacing some of the traditionally used structural materials. In view of this acceptance, development of robust analytical/numerical models is evident. It is through these models that the effect of shapes, sizes and location of second phase inclusions on the evolution of state variables and material properties in actual microstructures of heterogeneous materials can be investigated. Since the applied thermal and mechanical loads are at the structural level, models should also be capable of correlating the microstructural response with the overall macroscopic behavior. This implies the introduction of multiple scales in the computational model for accurate analysis.

A number of analytical micromechanical models have evolved within the framework of small deformation linear elasticity theory for heterogeneous materials. These models predict effective constitutive response at the macroscopic level from characteristics of microstructural behavior. Notable among them are models based on: (i) variational approach using extremum principles [see e.g. Hashin and Strikman (1963); Nemat-Nasser *et al.* (1993)]; (ii) probabilistic approach [see e.g. Chen and Acrivos (1978)]; (iii) self consistent schemes [see e.g. Hill (1965); Budiansky (1965)]; (iv) the generalized self consistent model [see e.g. Christensen and Lo (1979); Hori and Nemat-Nasser (1993)]. A cogent review of these models is presented in Mura (1987). These models follow the idea

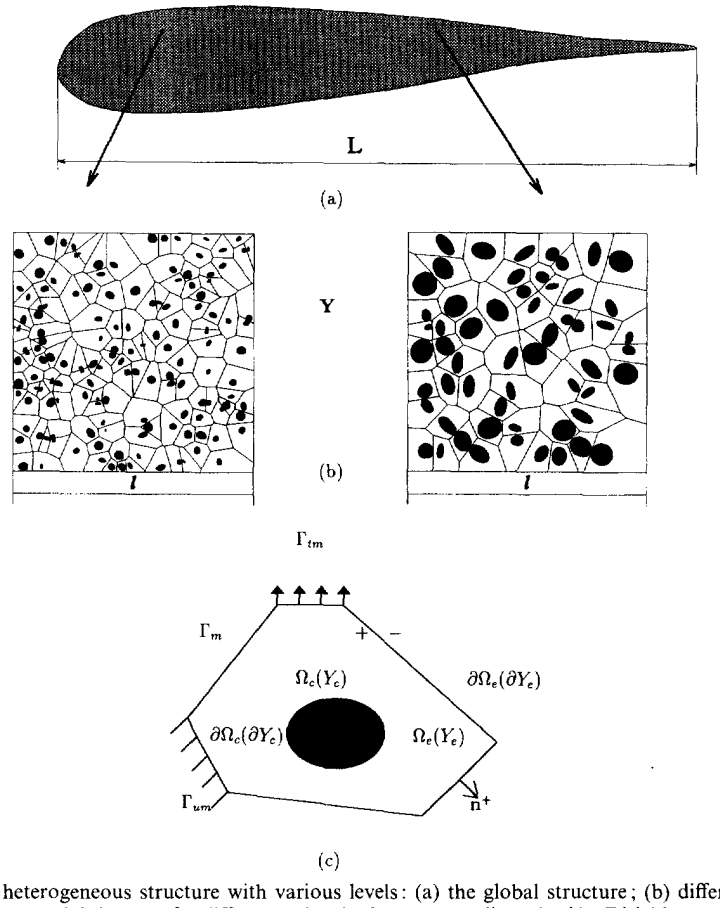


Fig. 1. A heterogeneous structure with various levels: (a) the global structure; (b) different representative material elements for different points in the structure discretized by Dirichlet tessellation; (c) a basic structural element represented by a Voronoi cell.

of equivalent inclusion methods based on eigenstrain formulation, originally proposed by Eshelby (1958). Though most of these analytical models are reasonably effective in predicting equivalent material properties for relatively simple geometries and low volume fraction of second phase inclusions, they are often incapable of depicting the evolution of stresses and strains in the microstructure. Arbitrary microstructural morphology, which are frequently encountered in actual heterogeneous materials, cannot be treated with these models. Constitutive response of the constituent phases are also somewhat restricted and predictions with large property mismatches are not very reliable.

In an attempt to overcome these limitations, *unit cell* models [see e.g. Bao *et al.* (1991); Tvergaard (1990); Christman *et al.* (1989)] using computational methods like the finite element method have become increasingly popular. These models generate effective material response and evolution through detailed discretization of a representative volume element (RVE) in the heterogeneous microstructure. Macroscopic periodicity conditions are assumed on the unit cells, i.e. the microstructure is assumed to be a periodic repetition of unit cells. Most of these models also make assumptions on local periodicity. Effectively, the local periodicity assumption reduces a *representative material element* (RME) to a *basic structural element* (BSE), thereby making the unit cells very simple. Despite their overall success, the unit cell methods suffer from a few drawbacks. While periodic spatial distribution is often useful to predict optimum properties, the fact remains that real heterogeneous structures seldom have periodic microstructures. Different global points [A and B in Fig. 1(a)], may have very different microstructural morphology. Also, micrographs obtained for actual materials often show arbitrariness in distribution, thereby making the assumption of local periodicity too restrictive. Shortcomings of these assumptions are

further enhanced in complex loading situations that cause nonhomogeneous structural deformation with nonlinearities. To circumvent these deficiencies, unit cell models should encompass large domains leading to enormously large computational models.

In the 1970s, an alternative mathematical theory originated for analysing characteristics of heterogeneous media and was called the *homogenization theory* by Benssousan *et al.* (1978) and Sanchez-Palencia (1980). This has proven to be a powerful technique for the analysis of physical systems in which two or more length scales naturally exist. These are the microscopic scale of inter-second phase spacing and the macroscopic scale characterizing overall dimensions of the structure. Through the use of asymptotic expansions of displacement and stress fields and appropriate variational principles, the homogenization methods can provide not only the effective (homogenized) material parameters, but also distributions of stresses and strains at the two levels. A prime advantage of this method over the unit cell approach is that it is not restricted to making assumptions of global periodicity, i.e. the structure can have different microstructures at different points. The analysis, however, makes the assumption of local periodicity through the introduction of spatially repeated microscopic cells. The finite element method has been successfully applied in conjunction with the homogenization theory for the analysis of linear elastic reinforced composites by Toledano and Murakami (1987), Guedes and Kikuchi (1991) and Devries *et al.* (1989). Computer simulations in these studies have provided the global response in the macroscopic structure through averaged stress/strain fields as well as the microstructural behavior through a depiction of local stress/strain fields. The homogenization method has been also implemented for finite deformation elasto-plasticity problems by Guedes and Kikuchi (1990). Most of these studies have, however, made assumptions of very simple microscopic cells, thereby identifying RMEs with simple shaped BSEs. Experiments with actual micrographs with arbitrary dispersion, show that material deformation is considerably influenced by its microstructural morphology. Current studies with the homogenization method have not been totally successful in depicting these characteristics. A recent study by Fish and Wagiman (1992) has superposed microscopic displacement fields on macroscopic fields to overcome this limitation for locally non-periodic heterogeneous materials.

In the quest of developing a computational model for arbitrary heterogeneous materials, Ghosh and coworkers [Ghosh and Mukhopadhyay (1991, 1993); Ghosh and Liu (1994); Ghosh and Mallett (1994); Ghosh and Moorthy (1994)] have innovated a material based *Voronoi cell finite element method* (VCFEM). The VCFEM mesh evolves naturally from a heterogeneous microstructure by *Dirichlet tessellation*. Tessellation of a microstructural material element (RME) discretizes the domain into a network of multisided convex "Voronoi" polygons containing one second phase inclusion at most, as shown in Fig. 1(b). A robust mesh generator to create these polygons based on shape, size and location of the heterogeneities has been developed by Ghosh and Mukhopadhyay (1991). In their work the multi-phase Voronoi polygons, identified with the basic structural elements as depicted in Fig. 1(c), are directly treated as elements in the finite element method. Element formulations have been developed for linear elastic problems in Ghosh and Mukhopadhyay (1993), micropolar thermo-elasticity problems in Ghosh and Liu (1994) and for elastic–plastic problems in Moorthy *et al.* (1994) and Ghosh and Moorthy (1994). Tessellation methods have been used by Richmond and coworkers [Spitzig *et al.* (1985); Brockenbrough *et al.* (1992); Fridy *et al.* (1992)] in conjunction with quantitative characterization of micrographs obtained by automatic image analysis systems. The Voronoi cell finite element method has the potential for establishing a direct correlation between techniques of quantitative metallography for actual heterogeneous materials microstructures and their stress/deformation analysis.

In the present paper, a coupled multiscale two-dimensional computational model is developed for heterogeneous linear elastic structures. The asymptotic homogenization theory provides a basis for consistently transferring information between the two levels, namely:

(a) microscopic information to the macro-level to generate global homogenized

coefficients and residual stresses at each sampling point of the macroscopic finite element model;

(b) macroscopic information to the micro-level after global analysis to compute the distribution of stresses and strains in the microstructure.

The Voronoi cell finite element method is implemented for analysing microstructures, which may consist of arbitrary dispersions of second phase inclusions in the matrix. A conventional displacement based FEM code is used in global analysis at the level of overall structural geometry and applied loads. Effect of shapes, sizes and locations of microscopic inclusions on the structural performance and the evolution of microstructural stresses and strains are studied through a variety of examples.

## 2. MICROSTRUCTURAL MODELING WITH THE VORONOI CELL FINITE ELEMENT METHOD

Voronoi cells make rather unconventional elements due to the fact that different elements can have a different number of sides. Application of the displacement finite element method to an element with $n$ nodes runs into difficulty when $n > 4$, because it is impossible to ensure inter-element displacement compatibility with $n$-term polynomial representations. Additionally, rank deficiencies in the stiffness matrix may result. These difficulties in representing Voronoi cells as conforming elements have been averted by invoking the assumed stress hybrid method introduced by Pian (1964). In this method, element stiffness matrices are derived by assuming compatible displacement fields along inter-element boundaries and a stress distribution in the interior of each element. Since interpolation of displacement field is only needed along the element boundary, it is appropriate for $n$-sided polygonal elements having a varying number of nodes. Stress polynomials are chosen to satisfy equilibrium within the element. The element formulation is based on the principle of minimum complementary energy. Details of this formulation may be found in Ghosh and Mukhopadhyay (1993).

The complimentary energy functional for a Voronoi element is of the form

$$\Pi_e^{\mathrm{E}} = -\int_{\Omega_e} \mathrm{B}(\boldsymbol{\sigma})\,\mathrm{d}\Omega + \int_{\partial\Omega_e} \boldsymbol{\sigma}\cdot\mathbf{n}\cdot\mathbf{u}\,\mathrm{d}\,\partial\Omega - \int_{\Gamma_{t_e}} \bar{\mathbf{t}}\cdot\mathbf{u}\,\mathrm{d}\Gamma, \tag{1}$$

where $\boldsymbol{\sigma}$ is the equilibriated stress field in the element domain $\Omega_e$, $\mathbf{u}$ is the compatible displacement field on the element boundary $\partial\Omega_e$ with an outward normal $\mathbf{n}$, $\bar{\mathbf{t}}$ is the prescribed traction field on $\Gamma_{t_e}$, the element boundary that coincides with global traction boundary. For linear elastic problems, the complimentary energy density $B(\boldsymbol{\sigma})$ takes the form

$$B(\boldsymbol{\sigma}) = \tfrac{1}{2}\{\boldsymbol{\sigma}\}^{\mathrm{T}}[\mathbf{S}]\{\boldsymbol{\sigma}\}, \tag{2}$$

where $S_{ijkl}$ are components of the elastic compliance tensor. In applying the finite element method, the assumed stress field need not be continuous across the inter-element boundaries but equilibrium must be maintained with surface tractions $t_i$ defined by

$$t_i = \sigma_{ij} n_j. \tag{3}$$

In the application of variational principles, the equilibriating stress field is expressed as a polynomial in the interior of the element as

$$\{\boldsymbol{\sigma}\} = [\mathbf{P}]\{\boldsymbol{\beta}\} \quad \text{in} \quad \Omega_e, \tag{4}$$

where, for two-dimensional problems, $\{\boldsymbol{\sigma}\}$ is a column vector of three stress components, $\{\boldsymbol{\beta}\}$ is a column of $m$ undetermined stress coefficients $\beta_1, \beta_2 \ldots \beta_m$ and $[\mathbf{P}]$ is a $3 \times m$ matrix containing functions of coordinates $x, y$ corresponding to the chosen polynomial. The

prescribed boundary displacements $\{\mathbf{u}\}$ can be interpolated from the generalized displacement $\{\mathbf{q}\}$ at the nodes, in the form

$$\{\mathbf{u}\} = [\mathbf{L}]\{\mathbf{q}\} \quad \text{in} \quad \partial\Omega_e, \tag{5}$$

where elements of the matrix $[\mathbf{L}]$ are functions of boundary coordinates. Stationarity of $\Pi_e^{\mathrm{E}}$ with respect to stress coefficients, i.e.

$$\frac{\partial \Pi_e^{\mathrm{E}}}{\partial \beta_i} = 0 \quad \text{for} \quad i = 1, 2 \ldots m, \tag{6}$$

yields

$$[\mathbf{H}]\{\boldsymbol{\beta}\} = [\mathbf{G}]\{\mathbf{q}\}, \tag{7}$$

where

$$[\mathbf{H}] = \int_{\Omega_e} [\mathbf{P}]^{\mathrm{T}}[\mathbf{S}][\mathbf{P}]\, \mathrm{d}\Omega$$

$$[\mathbf{G}] = \int_{\partial\Omega_e} [\mathbf{P}]^{\mathrm{T}}\{\mathbf{n}\}[\mathbf{L}]\, \mathrm{d}\Gamma.$$

Substitution of $\{\boldsymbol{\beta}\}$ in the expression for complementary strain energy $\Pi^{\mathrm{E}} = (\Sigma_e \Pi_e^{\mathrm{E}})$ for the entire domain and setting the first variation $\delta\Pi^{\mathrm{E}} = 0$ gives

$$[\mathbf{K}]\{\mathbf{q}\} = \{\bar{\mathbf{f}}\}, \tag{8}$$

where the element stiffness matrix is written as

$$[\mathbf{K}] = [\mathbf{G}]^{\mathrm{T}}[\mathbf{H}]^{-1}[\mathbf{G}], \tag{9}$$

and the load vector is denoted as

$$\{\bar{\mathbf{f}}\} = \int_{\partial\Omega_t} \{\bar{\mathbf{t}}\}^{\mathrm{T}}\{\mathbf{L}\}\, \mathrm{d}\Gamma.$$

The stiffness matrix $[\mathbf{K}]$ will be rank deficient if its rank is less than $n-l$ where $n$ is the number of degrees of freedom and $l$ is the number of rigid body modes. The necessary condition for $[\mathbf{K}]$ to have sufficient rank is $m \geqslant n-l$, where $m$ is the number of independent $\beta$-stress coefficients. Furthermore, if the assumed polynomials are complete, rotational invariance of the stiffness matrix is assured. The interpolation matrix $[\mathbf{P}]$ can be readily obtained by assuming variable degree complete polynomials for the Airy's stress function in plane problems. For example, in two dimensions, stresses resulting from third-order polynomials with no body forces can be delineated as

$$\begin{Bmatrix} \sigma_{11} \\ \sigma_{22} \\ \sigma_{12} \end{Bmatrix} = \begin{bmatrix} 1 & x_2 & 0 & 0 & 0 & x_1 & 0 \\ 0 & 0 & 1 & x_1 & 0 & 0 & x_2 \\ 0 & 0 & 0 & 0 & 1 & -x_2 & -x_1 \end{bmatrix} \begin{Bmatrix} \beta_1 \\ \vdots \\ \beta_7 \end{Bmatrix}, \tag{10}$$

where the components are expressed in a rectangular Cartesian coordinate system $x_i$. In this case there are seven $\beta$-terms in the stress polynomial and, hence, the $[\mathbf{P}]$ matrix can be used for elements having up to five nodes. For elements with a higher number of nodes, it is necessary to increase the number of $\beta$-terms to get rank sufficiency of the stiffness matrix.

The matrix [**P**] corresponding to 12 and 18 $\beta$-terms are given in Ghosh and Mukhopadhyay (1993). The displacements on an element boundary can be interpolated by using a linear function. For the $i$th side of an element

$$\{\mathbf{u}\} = \begin{Bmatrix} u_1 \\ u_2 \end{Bmatrix} = [\mathbf{L}]\{\mathbf{q}\} = \begin{bmatrix} 1-a/l_i & 0 & a/l_i & 0 \\ 0 & 1-a/l_i & 0 & a/l_i \end{bmatrix} \begin{Bmatrix} q_{2i-1} \\ q_{2i} \\ q_{2i+1} \\ q_{2i+2} \end{Bmatrix}, \tag{11}$$

where $l_i$ is the length of side $i$, $a$ is the distance of a boundary point from the $i$th node and $\{\mathbf{q}\}$ corresponds to the generalized displacements at nodal points. The effectiveness of this formulation has been elucidated by numerical examples in Ghosh and Mukhopadhyay (1993) and Ghosh and Mallett (1994).

2.1. *Composite Voronoi finite elements with inclusions*

A composite Voronoi element formulation is developed for incorporating the effect of an embedded heterogeneity in the matrix of an element [see Fig. 1(c)]. The approach is based on the consideration of multiple phases through the introduction of traction continuity constraint at the matrix–inclusion interface. Along a bonded interface $\partial\Omega_e$, the stress and strain fields may be discontinuous, while the displacement and traction fields are assumed to be continuous. Discontinuity in the stress field is introduced by way of permitting jumps in the coefficients of the interpolating stress polynomials. The element complimentary energy functional $\Pi_e$ in eqn (1) is enhanced to ensure traction continuity constraint along the matrix–inclusion interface through the use of Lagrange multipliers. The traction compatibility condition on the matrix–inclusion interface can be expressed as

$$(\boldsymbol{\sigma}^m - \boldsymbol{\sigma}^c)\cdot\mathbf{n} = \mathbf{0} \quad \text{on} \quad \partial\Omega_e, \tag{12}$$

where $\mathbf{n}$ is the unit normal on $\partial\Omega_e$ into the matrix phase. Contrary to the homogeneous element, assumptions in a heterogeneous element are made on a stress field $\boldsymbol{\sigma}^m$ in the matrix part of the element $\Omega_e - \Omega_c$ and a stress field $\boldsymbol{\sigma}^c$ in the inclusion $\Omega_c$. These stress fields $\boldsymbol{\sigma}^m$ and $\boldsymbol{\sigma}^c$ are *a priori* assumed to satisfy equilibrium in $\Omega_e - \Omega_c$ and $\Omega_c$, respectively, but not necessarily on $\partial\Omega_e$. The discontinuous stress fields in an element may be expressed as

$$\{\boldsymbol{\sigma}\} = [\mathbf{P}]\{\boldsymbol{\beta} + L(\mathbf{x})\boldsymbol{\beta}'\} \quad \text{in} \quad \Omega_e, \tag{13}$$

where [**P**] is the interpolation matrix discussed previously, $\{\boldsymbol{\beta}'\}$ corresponds to the additional polynomial coefficients that project jumps in the stress values, and $L(\mathbf{x})$ is a position-dependent step function defined as

$$\begin{aligned} L(\mathbf{x}) &= 0 \quad \forall\, \mathbf{x} \in \Omega_e - \Omega_c \\ &= 1 \quad \forall\, \mathbf{x} \in \Omega_c. \end{aligned}$$

A compatible displacement field $\mathbf{u}'$ is also assumed on the interface $\partial\Omega_e$ as

$$\{\mathbf{u}'\} = [\mathbf{L}]\{\mathbf{q}'\} \quad \text{in} \quad \partial\Omega_e. \tag{14}$$

The element complimentary energy functional in eqn (1) is modified to accommodate the interface traction constraint (12) as

$$\Pi_e^C = \Pi_e - \int_{\partial\Omega_e} (\sigma^m - \sigma^c) \cdot \mathbf{n} \cdot \mathbf{u}' \, d\Omega \tag{15}$$

and, consequently, the total energy functional for the heterogeneous domain is expressed as

$$\Pi^C = \sum_e \Pi_e^C. \tag{16}$$

Variation of $\Pi_e^C$ with respect to $\mathbf{u}'$ yields the *a posteriori* traction compatibility condition (12). First variation of $\Pi_e^C$, with respect to the stress coefficients $\{\beta\}$ and $\{\beta'\}$, respectively, yields the following eqns (17) and (18) given as

$$[\mathbf{H}_e]\{\beta\} + [\mathbf{H}_c]\{\beta'\} = [\mathbf{G}_e]\{\mathbf{q}\} \tag{17}$$

$$[\mathbf{H}_c]\{\beta + \beta'\} = [\mathbf{G}_c]\{\mathbf{q}'\}, \tag{18}$$

where the matrices have the following forms:

$$[\mathbf{H}_e] = \int_{\Omega_e} [\mathbf{P}]^T [\mathbf{S}(\mathbf{x})][\mathbf{P}] \, d\Omega$$

$$[\mathbf{G}_e] = \int_{\partial\Omega_e} [\mathbf{P}]^T \{\mathbf{n}\}[\mathbf{L}] \, d\Gamma$$

$$[\mathbf{H}_c] = \int_{\Omega_c} [\mathbf{P}]^T [\mathbf{S}(\mathbf{x})][\mathbf{P}] \, d\Omega$$

$$[\mathbf{G}_c] = \int_{\partial\Omega_c} [\mathbf{P}]^T \{\mathbf{n}\}[\mathbf{L}] \, d\Gamma.$$

Equation (17) corresponds to the strain–displacement relations for the entire Voronoi element while eqn (18) gives the same relations for the inclusion alone. Additionally, variation of the total energy functional (16) with respect to $\{\mathbf{q}\}$ and $\{\mathbf{q}'\}$, respectively, yields the equations

$$[\mathbf{G}_e]^T \{\beta\} = \{\bar{\mathbf{f}}\} \tag{19}$$

$$[\mathbf{G}_c]^T \{\beta'\} = \{\mathbf{0}\}, \tag{20}$$

where

$$\{\bar{\mathbf{f}}\} = \int_{\partial\Omega_{t_e}} \{\bar{\mathbf{t}}\}^T \{\mathbf{L}\} \, d\Gamma.$$

Equation (19) corresponds to the inter-element traction reciprocity on $\partial\Omega_e - \Gamma_{t_e} - \Gamma_{u_e}$ where $\partial\Omega_e$ and $\Gamma_{t_e}$ are explained before and $\Gamma_{u_e}$ corresponds to that part of an element boundary where displacement is specified. Equation (20) implies the interface traction constraint given in eqn (12). Substituting eqns (17), (18) and (19) in eqn (15) yields a matrix equation of the form

$$\begin{bmatrix} \mathbf{K}_{11} & \mathbf{K}_{12} \\ \mathbf{K}_{12}^{\mathrm{T}} & \mathbf{K}_{22} \end{bmatrix} \begin{Bmatrix} \mathbf{q} \\ \mathbf{q}' \end{Bmatrix} = \begin{Bmatrix} \bar{\mathbf{f}} \\ \mathbf{0} \end{Bmatrix}. \tag{21}$$

In solving eqn (61) for the displacements and stresses, special care must be exercised to remove additional rigid body modes that are introduced by the interface displacement field $\{\mathbf{q}'\}$. Details of this procedure and the forms for [**K**]s are presented in Ghosh and Moorthy (1994).

## 3. HOMOGENIZATION METHOD WITH MICROSTRUCTURAL VCFEM

Consider an elastic composite body occupying a region $\Omega$, for which the microstructure constitutes spatially repeated heterogeneous base cells, as shown in Fig. 1(b). The body is subjected to a system of body forces **f**, surface tractions **t** on the boundary $\Gamma_t$, and prescribed displacement fields on the boundary $\Gamma_u$. In real heterogeneous materials, dimensions of the base cell of characteristic length $l$ are typically very small compared with the dimensions of the body of characteristic length $L$. The ratio of these microscopic and macroscopic scales $l/L$ is represented by a very small, positive number $\varepsilon$. When subjected to structural level loads and displacements, the resulting evolving variables, like deformation and stresses, vary from point to point in the macroscopic scale **x** of the body. Furthermore, a high level of heterogeneity in the microstructure causes a rapid variation of these variables in a small neighborhood $\varepsilon$ of the macroscopic point **x**. This corresponds to a microscopic scale $\mathbf{x}/\varepsilon$ and, consequently, all variables are assumed to exhibit dependence on both length scales, i.e. $\Phi^\varepsilon = \Phi(\mathbf{x}, \mathbf{x}/\varepsilon)$. The superscript $\varepsilon$ denotes the association of the function with the two length scales. In this notation, $\Omega^\varepsilon$ denotes a connected domain that extends the structural domain to its microstructure. Mathematically speaking,

$$\Omega^\varepsilon = \{\mathbf{x} \in \Omega : \Theta\left(\frac{\mathbf{x}}{\varepsilon}\right) = 1\}, \tag{22}$$

in which $\Theta(\mathbf{y}) = 1$ when **y** lies in the microscopic base cell. In most of the work on homogenization theory [see e.g. Guedes and Kikuchi (1991); Devries *et al.* (1989); Guedes (1990); Oleinik *et al.* (1992)], a periodic repetition of the microstructure about a macroscopic point **x** has been assumed, thereby making the dependence of the function on $\mathbf{y} = (\mathbf{x}/\varepsilon)$ periodic. This characteristic is often termed as **Y**-periodicity, where **Y** corresponds to a base cell. The elasticity tensor $E^\varepsilon_{ijkl}$ and compliance tensor $S^\varepsilon_{ijkl}$ in the connected domain are expressed as

$$E^\varepsilon_{ijkl}(\mathbf{x}) = E_{ijkl}(\mathbf{x}, \mathbf{y}) \tag{23}$$

$$S^\varepsilon_{ijkl}(\mathbf{x}) = S_{ijkl}(\mathbf{x}, \mathbf{y}) \quad \text{in} \quad \Omega^\varepsilon. \tag{24}$$

It is assumed that the stress and displacement fields satisfy the equilibrium equation, kinematic relation and the linear elastic constitutive relations, given as

$$\sigma^\varepsilon_{ij,j} = -f_i \quad \text{in} \quad \Omega^\varepsilon \tag{25}$$

$$e^\varepsilon_{kl} = \frac{1}{2}\left(\frac{\partial u^\varepsilon_k}{\partial x^\varepsilon_l} + \frac{\partial u^\varepsilon_l}{\partial x^\varepsilon_k}\right) \quad \text{in} \quad \Omega^\varepsilon \tag{26}$$

$$\sigma^\varepsilon_{ij} = E^\varepsilon_{ijkl} e^\varepsilon_{kl} \quad \text{in} \quad \Omega^\varepsilon, \tag{27}$$

where $\mathbf{u}^\varepsilon = \mathbf{u}^\varepsilon(\mathbf{x}, \mathbf{y})$ is a **Y**-periodic displacement field in **y**. Furthermore the boundary

conditions are assumed to satisfy the following equations on the prescribed traction and displacement boundaries, respectively:

$$\sigma_{ij}^{\varepsilon} n_j = t_i \quad \text{on} \quad \Gamma_t \tag{28}$$

$$u_i^{\varepsilon} = \bar{u}_i \quad \text{on} \quad \Gamma_u, \tag{29}$$

where $\mathbf{n}$ is the unit normal to the boundary. In homogenization theory, the $\mathbf{Y}$-periodic displacement field is approximated by an asymptotic expansion about a global coordinate $\mathbf{x}$ as

$$\mathbf{u}^{\varepsilon}(\mathbf{x}) = \mathbf{u}^0(\mathbf{x}, \mathbf{y}) + \varepsilon \mathbf{u}^1(\mathbf{x}, \mathbf{y}) + \varepsilon^2 \mathbf{u}^2(\mathbf{x}, \mathbf{y}) + \ldots, \qquad \mathbf{y} = \frac{\mathbf{x}}{\varepsilon}. \tag{30}$$

Noting that the spatial $\mathbf{x}$ derivative of any function depending on the two length scales is given as

$$\frac{\partial}{\partial x_i^{\varepsilon}} \left( \Phi\left(\mathbf{x}, \mathbf{y} = \frac{\mathbf{x}}{\varepsilon}\right) \right) = \frac{\partial \Phi}{\partial x_i} + \frac{1}{\varepsilon} \frac{\partial \Phi}{\partial y_i}, \tag{31}$$

the strain tensor may be expressed as

$$e_{kl}^{\varepsilon} = \frac{\partial u_k^{\varepsilon}}{\partial x_l^{\varepsilon}} = \frac{1}{\varepsilon} \frac{\partial u_k^0}{\partial y_l} + \left( \frac{\partial u_k^0}{\partial x_l} + \frac{\partial u_k^1}{\partial y_l} \right) + \varepsilon \left( \frac{\partial u_k^1}{\partial x_l} + \frac{\partial u_k^2}{\partial y_l} \right) + \ldots. \tag{32}$$

Substituting this in the constitutive relation (27), the stress field $\boldsymbol{\sigma}^{\varepsilon}$ can be expanded as

$$\sigma_{ij}^{\varepsilon} = \frac{1}{\varepsilon} \sigma_{ij}^0 + \sigma_{ij}^1 + \varepsilon \sigma_{ij}^2 + \varepsilon^2 \sigma_{ij}^3 \ldots, \tag{33}$$

where

$$\begin{aligned} \sigma_{ij}^0 &= E_{ijkl}^{\varepsilon} \frac{\partial u_k^0}{\partial y_l} \\ \sigma_{ij}^1 &= E_{ijkl}^{\varepsilon} \left( \frac{\partial u_k^0}{\partial x_l} + \frac{\partial u_k^1}{\partial y_l} \right) \\ \sigma_{ij}^2 &= E_{ijkl}^{\varepsilon} \left( \frac{\partial u_k^1}{\partial x_l} + \frac{\partial u_k^2}{\partial y_l} \right). \end{aligned} \tag{34}$$

Putting the expansion of $\sigma_{ij}^{\varepsilon}$ (33) in the equilibrium eqn (25), and setting each coefficient of $\varepsilon^i$ ($i = -2, -1, 0, 1, 2 \ldots$) to zero, results in the following set of equations:

$$\frac{\partial \sigma_{ij}^0}{\partial y_j} = 0 \tag{35}$$

$$\frac{\partial \sigma_{ij}^1}{\partial y_j} + \frac{\partial \sigma_{ij}^0}{\partial x_j} = 0 \tag{36}$$

$$\frac{\partial \sigma_{ij}^2}{\partial y_j} + \frac{\partial \sigma_{ij}^1}{\partial x_j} + f_i = 0. \tag{37}$$

The first eqn (35) leads to the trivial value for $\sigma_{ij}^0$, and therefore $\mathbf{u}^0$ is only a function of $\mathbf{x}$, as shown in Devries *et al.* (1989), i.e.

$$\sigma_{ij}^0 = 0 \qquad \text{and} \qquad u_i^0 = u_i^0(\mathbf{x}). \tag{38}$$

Substituting this condition in eqn (36) leads to the $\mathbf{Y}$ domain equilibrium equation

$$\frac{\partial \sigma_{ij}^1}{\partial y_j} = 0. \tag{39}$$

In the expression for $\sigma_{ij}^1$ in eqn (34), the term $\partial u_k^0/\partial x_l$ is simply a constant with respect to the differential system $\mathbf{y}$. Due to linearity of the problem, $\sigma_{ij}^1$ and $u_i^1$ can be expressed in the following forms:

$$\sigma_{ij}^1 = \hat{\sigma}_{ij}^{kl}(\mathbf{y}) \frac{\partial u_k^0}{\partial x_l}, \qquad u_i^1 = \chi(\mathbf{y})_i^{kl} \frac{\partial u_k^0}{\partial x_l}, \tag{40}$$

where

$$\frac{\partial \hat{\sigma}_{ij}^{kl}(\mathbf{y})}{\partial y_j} = 0 \qquad \text{(microscopic equilibrium)} \tag{41}$$

$$\hat{\sigma}_{ij}^{kl}(\mathbf{y}) = E_{ijpm}^{\varepsilon}\left[T_{pm}^{kl} + \frac{\partial \chi_p^{kl}}{\partial y_m}\right] \qquad \text{(microscopic constitutive law)}. \tag{42}$$

In eqn (40), $\hat{\sigma}_{ij}^{kl}$ is a $\mathbf{Y}$-antiperiodic function and $\chi_i^{kl}$ is a $\mathbf{Y}$-periodic function, while $T_{ij}^{kl}$ in eqn (42) is a fourth-order identity tensor expressed as

$$T_{ij}^{kl} = \tfrac{1}{2}(\delta_{ik}\delta_{jl} + \delta_{il}\delta_{jk}). \tag{43}$$

The set of eqns (41) and (42) determine the vector $\chi(\mathbf{y})_k^{ij}$ to within an additive constant. Equation (39) may be solved for $\boldsymbol{\sigma}^1$ as

$$\sigma_{ij}^1(y) = E_{ijpm}^{\varepsilon}\left[T_{pm}^{kl} + \frac{\partial \chi_p^{kl}}{\partial y_m}\right]\frac{\partial u_k^0}{\partial x_l}. \tag{44}$$

For a $\mathbf{Y}$-periodic function $\Phi = \Phi(\mathbf{x}, \mathbf{y})$, the mean value may be defined as

$$\langle \Phi \rangle = \frac{1}{|\mathbf{Y}|}\int_{\mathbf{Y}} \Phi(\mathbf{x}, \mathbf{y})\, \mathrm{d}Y. \tag{45}$$

The mean of eqn (44) yields the macroscopic homogenized elastic coefficients in the form

$$E_{ijkl}^{\mathrm{H}} = \langle \hat{\sigma}_{ij}^{kl} \rangle = \frac{1}{|\mathbf{Y}|}\int_{\mathbf{Y}} \hat{\sigma}_{ij}^{kl}\, \mathrm{d}Y. \tag{46}$$

Taking the mean of eqn (37) in $\mathbf{Y}$ leads to an averaged the global equilibrium equation, given as

$$\frac{\partial \langle \sigma_{ij}^1 \rangle}{\partial x_j} + f_i = 0 \quad \text{in} \quad \Omega. \tag{47}$$

Note that the above eqn (47) is now valid for the macroscopic domain $\Omega$. Thus, in the macroscopic domain, the mean stress $\boldsymbol{\Sigma} = \langle \boldsymbol{\sigma}^1 \rangle$ and displacement fields $\mathbf{u}^0$ are the solutions to the elasticity problem delineated as

$$\begin{aligned} \frac{\partial \Sigma_{ij}}{\partial x_j} &= -f_i \quad \text{on} \quad \Omega \\ \Sigma_{ij} &= E^{\mathrm{H}}_{ijkl} \frac{\partial u_k^0}{\partial x_l} \\ \Sigma_{ij} n_j &= t_i \quad \text{on} \quad \Gamma_t \\ u_i^0 &= \bar{u}_i \quad \text{on} \quad \Gamma_u. \end{aligned} \tag{48}$$

3.1. *Coupling with microstructural VCFEM*

Homogenization method is now applied in conjunction with the Voronoi cell finite element method to couple global–local analysis. The VCFEM is used to model an arbitrary base cell which is identified with a microstructural representative element, as depicted in Fig. 1(b). The formulation presented in Section 2 is modified for identification of the VCFEM model as a true microstructural model in the homogenization method. Consequently, the base cell $\mathbf{Y}$ represents a VCFEM domain with a boundary $\partial\mathbf{Y}$. The base cell is now tessellated into $N$ Voronoi cell elements, each encompassing a region $Y_e$ and comprising of a boundary $\partial Y_e$ with outward normal $\mathbf{n}$ [Fig. 1(c)] and a composite boundary $\partial Y_c$. The equilibriated stress field is identified with the $\mathbf{Y}$-antiperiodic microscopic stress function $\hat{\boldsymbol{\sigma}}$ in eqns (41) and (42) with $\hat{\mathbf{e}}(\hat{\boldsymbol{\sigma}})$ as corresponding strain field in $Y_e$. Also, the element boundary displacement field is identified with the $\mathbf{Y}$-periodic microscopic displacement field $\boldsymbol{\chi}$, that is assumed to be compatible on the element boundary $\partial Y_e$ and $\boldsymbol{\chi}'$, the displacements on the composite interface $\partial Y_c$. In the absence of traction boundary conditions, complimentary energy functional in eqn (1) can be modified for each Voronoi element as

$$\Pi_e^{kl} = -\int_{Y_e} \tfrac{1}{2} S^e_{ijpm} \hat{\sigma}^{kl}_{ij} \hat{\sigma}^{kl}_{pm} \, \mathrm{d}Y + \int_{\partial Y_e} \chi_i^{kl} \hat{\sigma}^{kl}_{ij} n_j \, \mathrm{d}\partial Y + \int_{Y_e} T_{ij}^{kl} \hat{\sigma}_{ij}^{kl} \, \mathrm{d}Y - \int_{\partial Y_c} ((\hat{\sigma}_{ij}^{kl})^m - (\hat{\sigma}_{ij}^{kl})^c) n_j (\chi_i^{kl})' \, \mathrm{d}\partial Y, \tag{49}$$

where all variables have the same interpretations as stated before. Stationarity condition of the energy functional $\Pi_e^{kl}$ with respect to $\hat{\boldsymbol{\sigma}}$ yields the strain–displacement relations as a Euler equation

$$\hat{e}_{ij}^{kl} = S^e_{ijpm} \hat{\sigma}^{kl}_{pm} = T_{ij}^{kl} + \frac{\partial \chi_i^{kl}}{\partial y_j}. \tag{50}$$

It should be noted that eqn (50) is exactly the same as eqn (42), written with the elastic compliance tensor. The total energy functional for entire base cell domain is obtained by adding the element contributions as

$$\Pi^{kl}(\hat{\boldsymbol{\sigma}}, \boldsymbol{\chi}) = \sum_{e=1}^{N} \Pi_e^{kl}. \tag{51}$$

Stationarity of this functional with respect to displacements $\boldsymbol{\chi}$ results in the inter-element traction reciprocity condition

$$\hat{\boldsymbol{\sigma}} \cdot \mathbf{n}^{+} = -\hat{\boldsymbol{\sigma}} \cdot \mathbf{n}^{-} \quad \text{on} \quad \partial Y_e, \tag{52}$$

where superscript + and − denote values at opposite sides of the inter-element boundary $\partial Y_e$. Stationarity of this functional with respect to the displacement $\boldsymbol{\chi}'$ results in the interface traction constraint

$$\hat{\boldsymbol{\sigma}}^{m} \cdot \mathbf{n} = \hat{\boldsymbol{\sigma}}^{c} \cdot \mathbf{n} \quad \text{on} \quad \partial Y_c. \tag{53}$$

The complete microscopic boundary value problem is specified by:

(i) Euler equations (50), (52) and (53);
(ii) assumed equilibriated stress fields in $Y_e$ satisfying $\hat{\sigma}^{kl}_{ij,j} = 0$ in the absence of body forces;
(iii) assumed compatible displacement fields in $\partial Y_e$ and $\partial Y_c$
(iv) stress–strain relation $\hat{e}^{kl}_{ij} = S^{\varepsilon}_{ijpm}\hat{\sigma}^{kl}_{pm}$.

The scope of the present paper is confined to two-dimensional problems, for which the stresses and strains have three components each. Consequently, three separate VCFE analyses have to be conducted in applying the asymptotic homogenization method. Each analysis generates the microscopic response of a base cell for a given uniform state of a macroscopic strain component. A subscript $i$, where $i = 1, 2, 3$, has been used to distinguish these analyses in the ensuing treatment. For example, a subscript 1 corresponds to a uniform macroscopic strain $e^0_{11}$, 2 corresponds to $e^0_{22}$ and 3 corresponds to $e^0_{12}$. Using a vector form of parameters in eqn (49), the energy functional for the $i$th analysis can be rewritten as

$$(\Pi_e)_i = -\int_{Y_e} \tfrac{1}{2}\{\boldsymbol{\sigma}\}_i^{\mathrm{T}}[\mathbf{S}]\{\boldsymbol{\sigma}\}_i \,\mathrm{d}Y + \int_{\partial Y_e} \{\boldsymbol{\sigma}\}_i[\mathbf{n}]\,\{\boldsymbol{\chi}\}_i \,\mathrm{d}\partial Y + \int_{Y_e} \{\boldsymbol{\sigma}\}_i^{\mathrm{T}}\{\mathbf{T}\}_i \,\mathrm{d}Y - \int_{\partial Y_c} (\{\boldsymbol{\sigma}^m\} - \{\boldsymbol{\sigma}^c\})_i^{\mathrm{T}}[\mathbf{n}]\,\{\boldsymbol{\chi}'\}_i \,\mathrm{d}\partial Y_c, \tag{54}$$

where $\{\boldsymbol{\sigma}\}$ is a column of stress components $\{\hat{\sigma}^{kl}_{11}, \hat{\sigma}^{kl}_{22}, \hat{\sigma}^{kl}_{12}\}^{\mathrm{T}}$, $\{\boldsymbol{\chi}\}$ has the components $\{\chi^{kl}_1, \chi^{kl}_2\}^{\mathrm{T}}$ and $\{\mathbf{T}\}$ is a vector form of $T^{kl}_{ij}$ according to the definition in eqn (43). By making the same assumptions for the equilibriated stress field and compatible displacement field as in eqns (13) and (14), i.e.

$$\begin{aligned} \{\boldsymbol{\sigma}\}_i &= [\mathbf{P}]\,\{\boldsymbol{\beta} + L(\mathbf{x})\boldsymbol{\beta}'\}_i \quad \text{in} \quad Y_e \\ \{\boldsymbol{\chi}\}_i &= [\mathbf{L}]\{\mathbf{q}\}_i \quad \text{in} \quad \partial Y_e \\ \{\boldsymbol{\chi}'\}_i &= [\mathbf{L}]\{\mathbf{q}'\}_i \quad \text{in} \quad \partial Y_c \end{aligned} \tag{55}$$

and substituting in eqn (54), the element energy functional takes the form

$$(\Pi_e)_i = -\int_{Y_e} \tfrac{1}{2}\{\boldsymbol{\beta} + L(\mathbf{x})\boldsymbol{\beta}'\}_i^{\mathrm{T}}[\mathbf{P}]^{\mathrm{T}}[\mathbf{S}][\mathbf{P}]\{\boldsymbol{\beta} + L(\mathbf{x})\boldsymbol{\beta}'\}_i \,\mathrm{d}Y + \int_{\partial Y_e} \{\boldsymbol{\beta}\}_i^{\mathrm{T}}[\mathbf{P}]^{\mathrm{T}}[\mathbf{n}][\mathbf{L}]\{\mathbf{q}\}_i \,\mathrm{d}\partial Y + \int_{Y_e} \{\boldsymbol{\beta} + L(\mathbf{x})\boldsymbol{\beta}'\}_i^{\mathrm{T}}[\mathbf{P}]^{\mathrm{T}}\{\mathbf{T}\}_i \,\mathrm{d}Y + \int_{\partial Y_c} \{\boldsymbol{\beta}'\}_i^{\mathrm{T}}[\mathbf{P}]^{\mathrm{T}}[\mathbf{n}][\mathbf{L}]\{\mathbf{q}'\}_i \,\mathrm{d}\partial Y_c \tag{56}$$

or

$$(\Pi_e)_i = -\tfrac{1}{2}\{\boldsymbol{\beta}\}_i^{\mathrm{T}}[\mathbf{H}_e]\{\boldsymbol{\beta}\}_i - \{\boldsymbol{\beta}\}_i^{\mathrm{T}}[\mathbf{H}_c]\{\boldsymbol{\beta}'\}_i - \tfrac{1}{2}\{\boldsymbol{\beta}'\}_i^{\mathrm{T}}[\mathbf{H}_c]\{\boldsymbol{\beta}'\}_i + \{\boldsymbol{\beta}\}_i^{\mathrm{T}}[\mathbf{G}_e]\{\mathbf{q}\}_i + \{\boldsymbol{\beta}'\}_i^{\mathrm{T}}[\mathbf{G}_c]\{\mathbf{q}'\}_i + \{\boldsymbol{\beta}\}_i^{\mathrm{T}}\{\mathbf{D}\}_i + \{\boldsymbol{\beta}'\}_i^{\mathrm{T}}\{\mathbf{D}_c\}_i, \quad (57)$$

where $[\mathbf{H}_e]$, $[\mathbf{H}_c]$, $[\mathbf{G}_e]$ and $[\mathbf{G}_c]$ are defined in Section 2 and

$$\{\mathbf{D}\}_i = \int_{Y_e} [\mathbf{P}]^{\mathrm{T}}\{\mathbf{T}\}_i \, \mathrm{d}Y$$

$$\{\mathbf{D}_c\}_i = \int_{Y_c} [\mathbf{P}]^{\mathrm{T}}\{\mathbf{T}\}_i \, \mathrm{d}Y. \quad (58)$$

Stationarity of $(\Pi_e)_i$ with respect to $\{\boldsymbol{\beta}\}_i$, and $\{\boldsymbol{\beta}'\}_i$, respectively yield

$$[\mathbf{H}_e]\{\boldsymbol{\beta}\}_i + [\mathbf{H}_c]\{\boldsymbol{\beta}'\}_i = [\mathbf{G}_e]\{\mathbf{q}\}_i + \{\mathbf{D}\}_i$$
$$[\mathbf{H}_c]\{\boldsymbol{\beta}+\boldsymbol{\beta}'\}_i = [\mathbf{G}_c]\{\mathbf{q}'\}_i + \{\mathbf{D}_c\}_i. \quad (59)$$

Showing eqn (59), $\{\boldsymbol{\beta}\}_i$ and $\{\boldsymbol{\beta}'\}_i$ are obtained as

$$\{\boldsymbol{\beta}\}_i = [\mathbf{H}_m]^{-1}([\mathbf{G}_e]\{\mathbf{q}\}_i - [\mathbf{G}_c]\{\mathbf{q}'\}_i + \{\mathbf{D}\}_i - \{\mathbf{D}_c\}_i)$$
$$\{\boldsymbol{\beta}'\}_i = ([\mathbf{H}_c]^{-1} + [\mathbf{H}_m]^{-1})([\mathbf{G}_c]\{\mathbf{q}'\}_i + \{\mathbf{D}_c\}_i) - [\mathbf{H}_m]^{-1}([\mathbf{G}_e]\{\mathbf{q}\}_i + \{\mathbf{D}\}_i). \quad (60)$$

Substitution of $\{\boldsymbol{\beta}\}_i$ and $\{\boldsymbol{\beta}'\}_i$ in the energy $\Pi = (\Sigma_e \Pi_e)$ for the entire domain, and setting first variation $\delta\Pi = 0$, gives

$$\begin{bmatrix} \mathbf{K}_{11} & \mathbf{K}_{12} \\ \mathbf{K}_{12}^{\mathrm{T}} & \mathbf{K}_{22} \end{bmatrix} \begin{Bmatrix} \mathbf{q} \\ \mathbf{q}' \end{Bmatrix} = \begin{Bmatrix} \bar{\mathbf{f}}_1 \\ \bar{\mathbf{f}}_2 \end{Bmatrix}, \quad (61)$$

where $[\mathbf{K}]$ are given in Ghosh and Moorthy (1994) and the load vector is given as

$$\{\bar{\mathbf{f}}_1\}_i = -[\mathbf{G}_e]^{\mathrm{T}}[\mathbf{H}_m]^{-1}(\{\mathbf{D}\}_i - \{\mathbf{D}_c\}_i)$$
$$\{\bar{\mathbf{f}}_2\}_i = -[\mathbf{G}_c]^{\mathrm{T}}([\mathbf{H}_m]^{-1} + [\mathbf{H}_c]^{-1})\{\mathbf{D}_c\}_i + [\mathbf{G}_c]^{\mathrm{T}}[\mathbf{H}_m]^{-1}\{\mathbf{D}\}_i. \quad (62)$$

The stiffness matrix $[\mathbf{K}]$ in eqn (61) is independent of the macroscopic strain field. Solution of eqns (60) and (61) yields the values of $\{\boldsymbol{\beta}\}_i$, $\{\boldsymbol{\beta}'\}_i$, $\{\mathbf{q}\}_i$ and $\{\mathbf{q}'\}_i$ which are then substituted into eqn (55) for the microscopic stress functions $\hat{\sigma}_{11}$, $\hat{\sigma}_{22}$ and $\hat{\sigma}_{12}$. The mean value of these functions are obtained from eqn (46) to generate the homogenized elastic coefficients $[\mathbf{E}]^{\mathrm{H}}$.

The homogenized elastic problem of eqn (48) can then be solved to get the macroscopic stress and strain fields $\{\boldsymbol{\Sigma}\}$ and $\{\mathbf{e}^0\}$, respectively. At a given point $\mathbf{x}$ in the macroscopic domain $\Omega$, the microscopic stress $\{\boldsymbol{\sigma}^1\}(\mathbf{x}, \mathbf{y})$ is calculated by using eqn (40) in a matrix form as

$$\{\boldsymbol{\sigma}^1\} = [\mathbf{P}]\,[\{\boldsymbol{\beta} + L(\mathbf{x})\{\boldsymbol{\beta}'\}\}_1 \{\boldsymbol{\beta} + L(\mathbf{x})\{\boldsymbol{\beta}'\}\}_2 \{\boldsymbol{\beta} + L(\mathbf{x})\{\boldsymbol{\beta}'\}\}_3]\{\mathbf{e}^0\}. \quad (63)$$

### 3.2. *Numerical implementation*

A number of numerical details have to be considered in the construction of a multiple scale computational model using the microstructural VCFEM model. In this section, a few salient features are discussed.

*Incorporating the periodicity boundary condition.* An essential step in computing the homogenized material properties for a base cell is to ensure repeatability boundary conditions. Irrespective of the shape and size of the base cell, this condition must be enforced

to represent periodic displacements of the microstructural boundary. As an example, if the base cell is a square, identical displacement functions must be specified for corresponding nodes (equidistant from a coordinate axis) on opposite edges. Implementing the repeatability boundary condition for a regular finite element mesh is straightforward, since a uniform mesh can be generated to have the correspondence between boundary nodes on opposite faces. However boundary nodes generated by Dirichlet tessellation in creating the Voronoi mesh are, in general, quite arbitrary and such a correspondence cannot be easily identified. A method which involves the representation of nodal boundary displacements by a suitable polynomial function is thereby implemented for enacting the repeatability conditions. In the tessellation method, a $(p-1)$th order polynomial is chosen for the displacements, where $p$ corresponds to the highest number of boundary nodes between the two opposite faces. That is, if one face has five nodes while the opposite side consists of six nodes, a fifth-order polynomial function is chosen. The edge nodal displacements are then written as

$$\begin{aligned} u_1 &= a_0 + a_1 x_1 + a_2 x_1^2 + a_3 x_1^3 + a_4 x_1^4 + a_5 x_1^5 \\ v_1 &= b_0 + b_1 y_1 + b_2 y_1^2 + b_3 y_1^3 + b_4 y_1^4 + b_5 y_1^5 \\ u_2 &= a_0 + a_1 x_2 + a_2 x_2^2 + a_3 x_2^3 + a_4 x_2^4 + a_5 x_2^5 \\ v_2 &= b_0 + b_1 y_2 + b_2 y_2^2 + b_3 y_2^3 + b_4 y_2^4 + b_5 y_2^5 \\ &\vdots \end{aligned} \tag{64}$$

where $u_1, v_1, u_2, v_2 \ldots$ are nodal displacements and $x_1, y_1, x_2, y_2 \ldots$ are boundary coordinates. These lead to displacement constraints that are implemented in the matrix equations prior to solving. It should be noted, that the polynomial representation in enforcing periodic boundary conditions effectively replaces the assumed displacement functions (55) for nodes on the domain boundary. This method has been very effective in enforcing the repeatability conditions.

*The macroscopic finite element model.* After calculating the homogenized material coefficients at a given macroscopic point $\mathbf{x}$ by VCFEM, the homogenization method requires the solution of the global problem given in eqn (48) with a macroscopic finite element model. In this work, the commercial code ANSYS is used for this purpose. Orthotropic elastic homogenized coefficients calculated from VCFEM are input as material properties in the ANSYS input file. Solution of the global problem yields the values of macroscopic displacements $\mathbf{u}^0$ and stress and strain fields $\{\boldsymbol{\Sigma}\}$ and $\{\mathbf{e}^0\}$, respectively.

*Evolution of variables in the microstructure.* Following the global solution, global strain $\{\mathbf{e}^0\}$ and the $\{\boldsymbol{\beta}\}_1$, $\{\boldsymbol{\beta}\}_2$ and $\{\boldsymbol{\beta}\}_3$ parameters are used to calculate the microscopic stress $\{\boldsymbol{\sigma}^1\}$. An advantage of VCFEM over conventional FEM models is that once the $\{\boldsymbol{\beta}\}_i$s are known, microscopic stresses can be very easily computed at any point in the microstructure using eqn (63).

## 4. NUMERICAL EXAMPLES

The numerical examples are subdivided into two parts. In the first part, results obtained from the VCFEM based homogenization method are compared with established numerical results of Fish and Wagiman (1992), Guedes (1990) and experimental results of Lynch (1975), and also with the results of a Galerkin finite element model based homogenization program (HOMO2D), developed from the work by Guedes (1990). In the second part, the effect of size, shape, orientation and location of the heterogeneities on the macroscopic and microscopic variables are examined by the VCFEM based homogenization program.

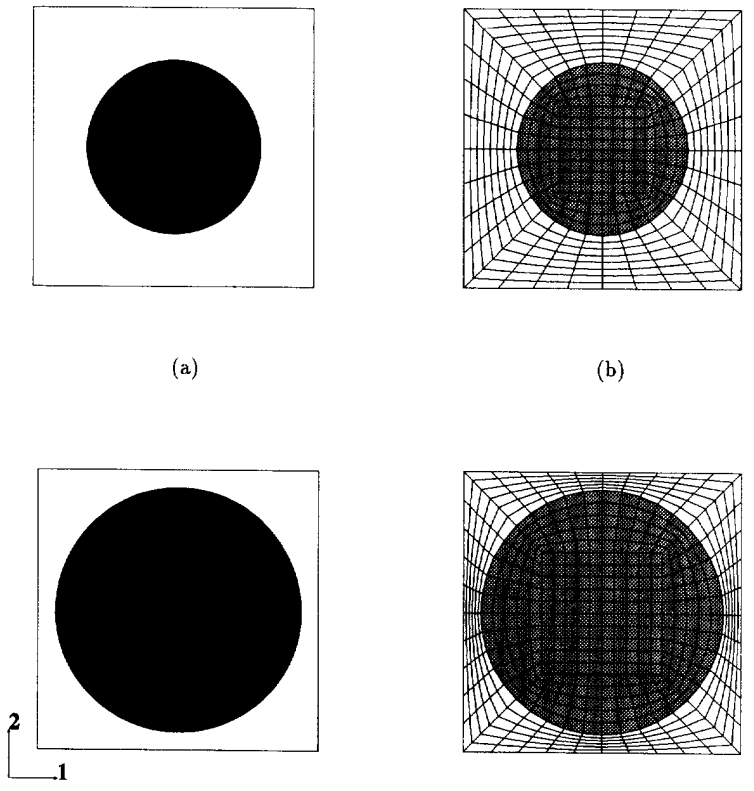


Fig. 2. Base cell with a single circular inclusion : (a) and (c) VCFEM mesh for 30% and 60% volume fractions ; (b) and (d) HOMO2D mesh for 30% and 60% volume fractions.

4.1. *Validation of the homogenization model*

In testing the accuracy of the VCFEM based homogenization model, two different sets of variables are checked. The first is the predicted values of homogenized material constants for a given base cell in the pre-processing part of the module, while the second corresponds to verification of stress distribution in the microstructure, following the solution of the macroscopic problem.

*Example* 1. In this example, homogenized coefficients are evaluated for microstructural cells containing different volume fractions (30, 40, 50, 60%) and distributions of circular inclusions. Isotropic constituent material properties are specified for a boron–aluminum composite system as

Boron fiber :

Young's modulus ($E_c$) : 400 GPa

Poisson ratio ($\nu_c$) : 0.3

Aluminum matrix :

Young's modulus ($E_m$) : 72.0 GPa

Poisson ratio ($\nu_m$) : 0.3333.

Results presented in Guedes (1990) are also for this material. Two distinct distributions are considered in this example. In one case, the base cell consists of a centrally located single circular fiber, the diameter of which is changed to correspond to various volume fractions. Figure 2 is a depiction of the VCFEM mesh and the Galerkin FEM mesh (HOMO2D) for two different volume fractions (30% and 60%) of this base cell. It should be noted that the VCFE model in this case consists of a single composite element. Convergence of this model is tested by conducting numerical experiments with 18 and 25 $\{\boldsymbol{\beta}\}$ parameters for the stress

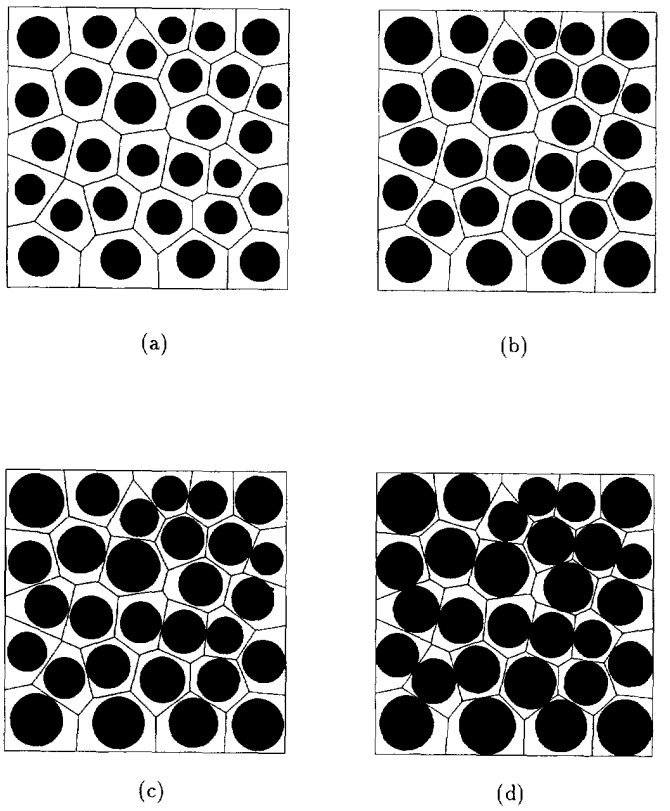


Fig. 3. Base cell with random dispersion of circular inclusion of different volume fractions: (a) 30%; (b) 40%; (c) 50%; (d) 60%.

interpolation in eqn (4). For the HOMO2D model, 448 (for 30%, 40%), 416 (for 50%) and 540 (for 60%) QUAD4 elements are used to discretize the base cell. In the other case, a random dispersion of circular fibers of different volume fractions constitute the microstructure. This microstructure has been modeled only by VCFEM, where the Voronoi elements consist of a single inclusion each. The corresponding Voronoi cell meshes for different volume fractions are shown in Fig. 3.

Homogenized material constants of the base cell are conducted for an orthotropic material characteristic under plane stress conditions. Predictions of VCFEM and HOMO2D are compared with results in Guedes (1990) and an experimental result by Lynch (1975). These comparisons for the Young's modulus in the one-direction ($E_1$) are shown in Fig. 4. The results show very good agreement between VCFEM and HOMO2D results, even though the number of elements in the HOMO2D mesh was orders of magnitude larger than the VCFEM mesh (only one element for the single inclusion). Furthermore, the VCFEM results converged rapidly to the HOMO2D results with increased $\{\boldsymbol{\beta}\}$ parameters. Discrepancy with the results in Guedes (1990), which exhibit slightly higher values, may be accounted for by the fact that the latter was essentially a three-dimensional analysis. Values of the homogenized constant ($E_1$) for the randomly dispersed microstructure are lower than those for the single inclusion but are closer to the experimental results of Lynch (1975). This indicates that homogenized properties derived for random microstructures are in better agreement with real materials.

*Example* 2. In this example, homogenized coefficients as well as stress distributions in the microstructure are evaluated by VCFEM and compared with results from HOMO2D and also of Fish and Wagiman (1992). Two representative material elements, consisting of short and long fibers with rectangular cross-sections are considered. The material properties are for a boron–aluminum composite system, with constituent properties

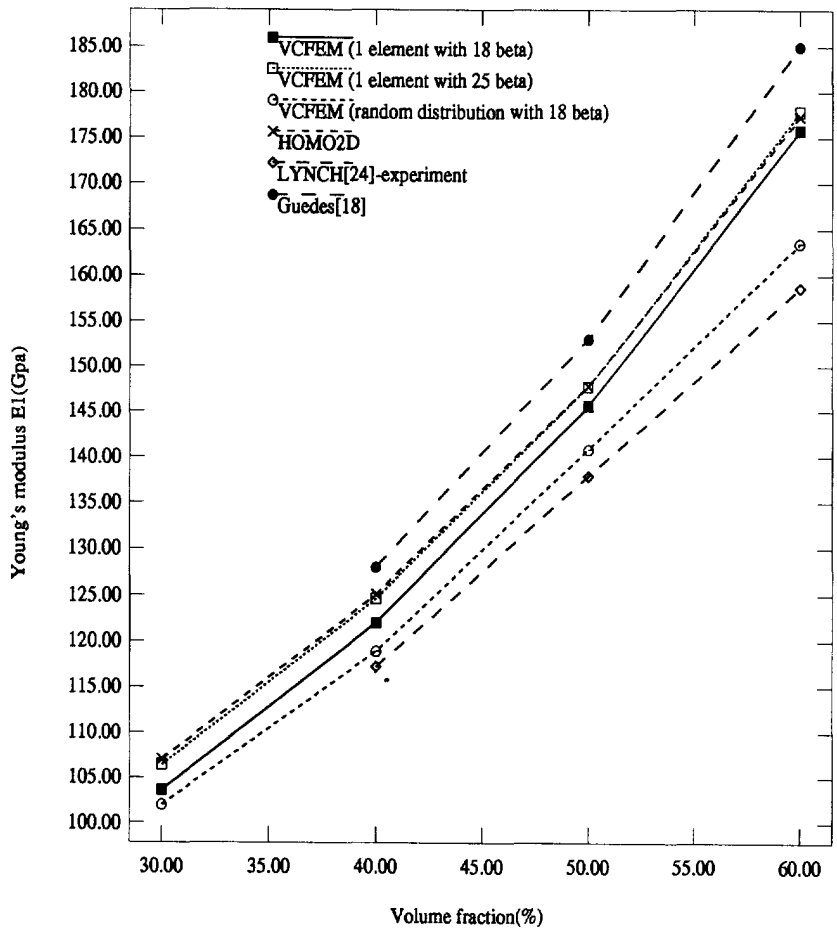


Fig. 4. Homogenized material properties with different volume fractions.

Boron fiber:

Young's modulus ($E_c$): 400 GPa

Poisson ratio ($v_c$): 0.2

Aluminum matrix:

Young's modulus ($E_m$): 72.5 GPa

Poisson ratio ($v_m$): 0.33.

Dimensions of the heterogeneities in the base cells are shown in Fig. 5. For the short fiber inclusions, the volume fraction of heterogeneities is 0.375, while that for the long fiber is 0.5. The VCFEM and HOMO2D meshes for these problems are depicted in Fig. 5. For the short fiber, the VCFEM consists of four elements and for the long fiber case, only one element is required. The HOMO2D mesh consists of 1600 elements for both cases. The number of $\{\beta\}$ parameters for the stress interpolation in the VCFEM is 18. Table 1 shows a comparison of homogenized material properties of short fiber base cell between VCFEM results and those by HOMO2D, a global–local FEM analysis by Fish and Wagiman (1992) and a self consistent model by Hashin (1970). In this case homogenized material properties calculated by VCFEM are slightly different to those from HOMO2D and Fish and Wagiman (1992). The small differences [E1111 (2%), E2222 (7.5%), E1212 (0.8%), E1122 (5%)] are acceptable, considering that large degrees of freedom are necessary for the comparison models. It is expected that higher order stress interpolations would improve the agreement. The agreement is even better for the long fiber base cell, as given in Table 2. It can be generally said that the results by HOMO2D converged to the VCFEM results with increasing mesh refinement.

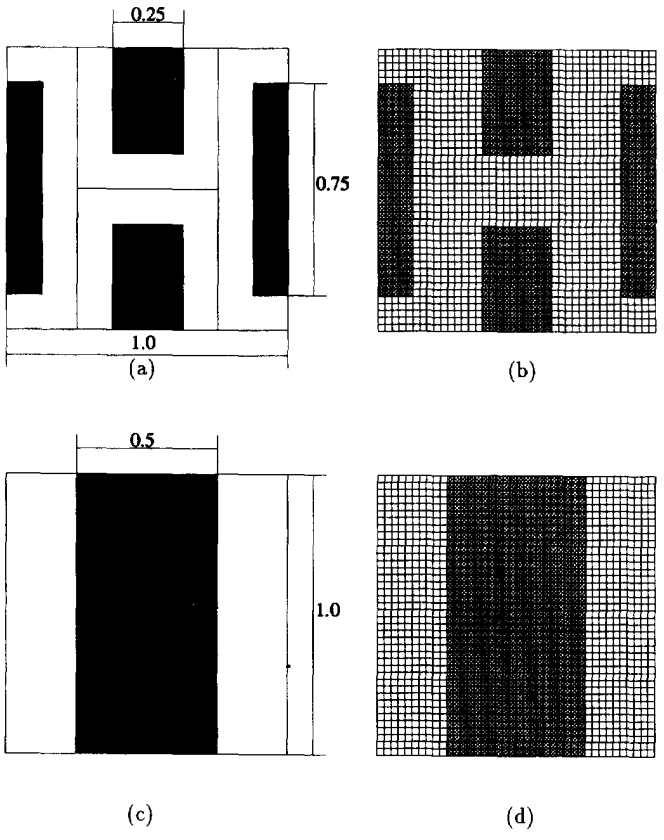


Fig. 5. Microstructure with rectangular heterogeneities: (a) short fiber mesh for VCFEM; (b) short fiber mesh for HOMO2D; (c) long fiber mesh for VCFEM; (d) long fiber mesh for HOMO2D.

The macroscopic structure solved with these microstructures is a thin composite plate with a centered hole. Because of symmetry only a quarter of the plate is modeled. The geometry, loading and boundary conditions are shown in Fig. 6. Dimensions of the plate are height ($h = 1.5$), width ($w = 1.0$) and radius of hole ($c = 0.1$); $c/w$ is chosen to be 0.1. The value of applied pressure is set to 1.0. The maximum macroscopic stresses in the structure for the two different microstructures at a point A (lower left corner), are presented in Table 3. Excellent agreement is obtained between VCFEM and HOMO2D. Figures 7 and 8 illustrate the macroscopic stress distributions and the distribution in the microstructure at

Table 1. Comparison of homogenized material properties for short fiber model

| | VCFEM | HOMO2D | Fish and Wagiman (1992) | Self consistent |
|---|---|---|---|---|
| E1111 (GPa) | 118.807 | 122.4 | 122.457 | 132.491 |
| E2222 (GPa) | 139.762 | 151.2 | 151.351 | 205.753 |
| E1212 (GPa) | 42.440 | 42.10 | 42.112 | 51.384 |
| E1122 (GPa) | 38.052 | 36.23 | 36.191 | 36.191 |

Table 2. Comparison of homogenized material properties for long fiber model

| | VCFEM | HOMO2D | Fish and Wagiman (1992) | Self consistent |
|---|---|---|---|---|
| E1111 (GPa) | 136.137 | 136.1 | 136.147 | 165.548 |
| E2222 (GPa) | 245.810 | 245.8 | 245.81 | 247.575 |
| E1212 (GPa) | 46.8498 | 46.85 | 46.85 | 64.887 |
| E1122 (GPa) | 36.076 | 36.08 | 36.076 | 42.048 |

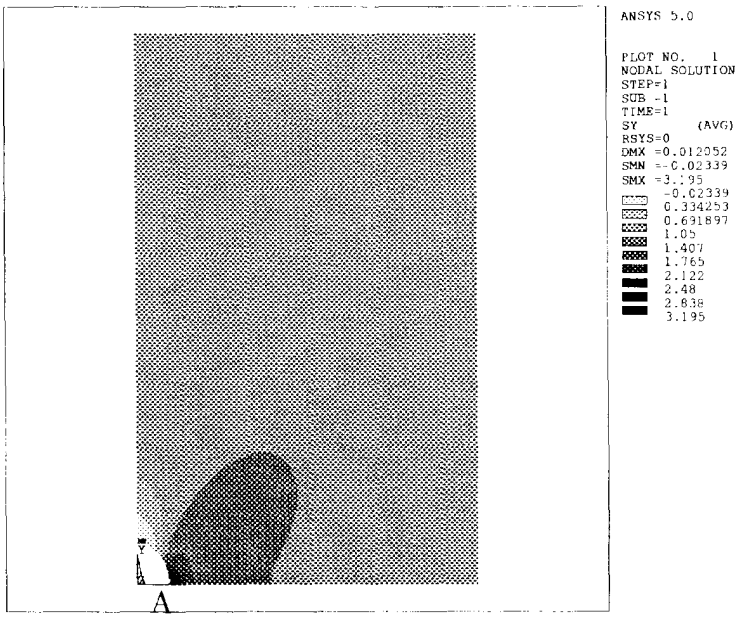


(a)

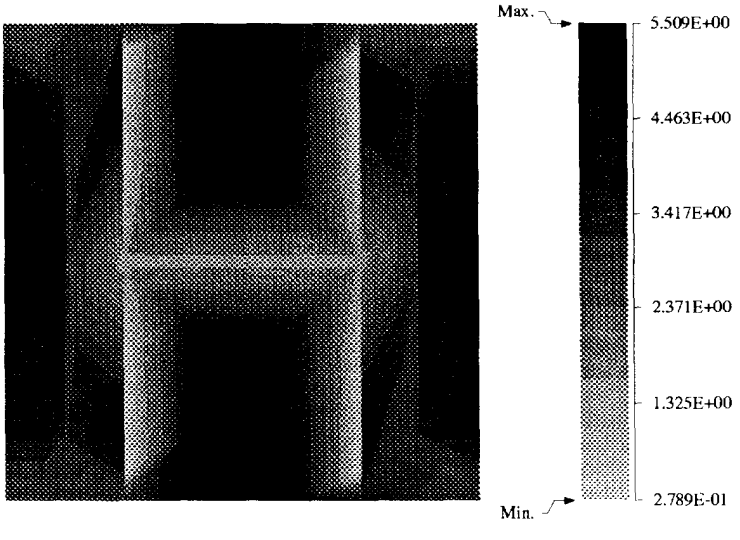


(b)

Fig. 7. Stress ($\sigma_y$) distribution for a short fiber microstructure: (a) macroscopic distribution: (b) microscopic distribution at A.

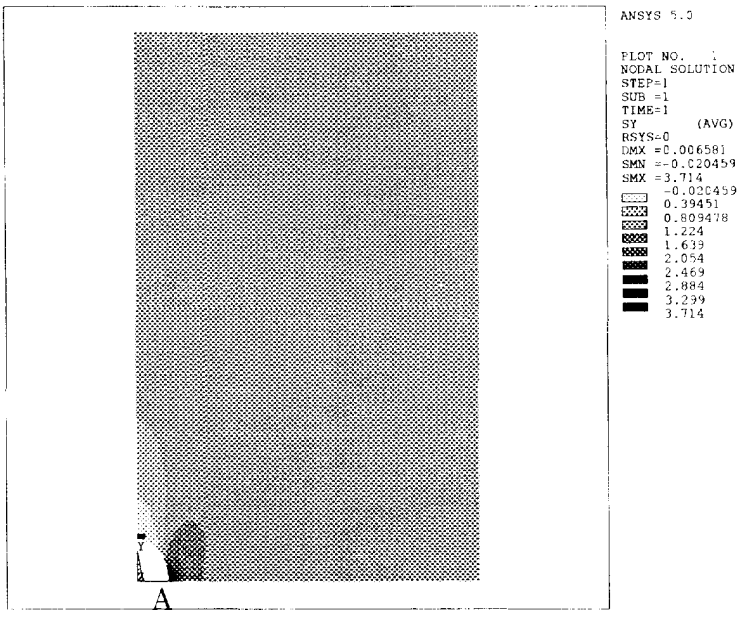


(a)

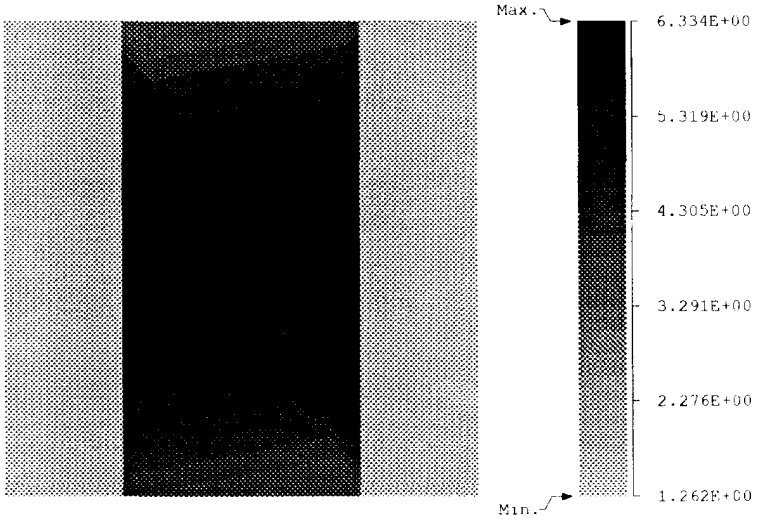


(b)

Fig. 8. Stress ($\sigma_y$) distribution for a long fiber microstructure: (a) macroscopic distribution; (b) microscopic distribution at A.

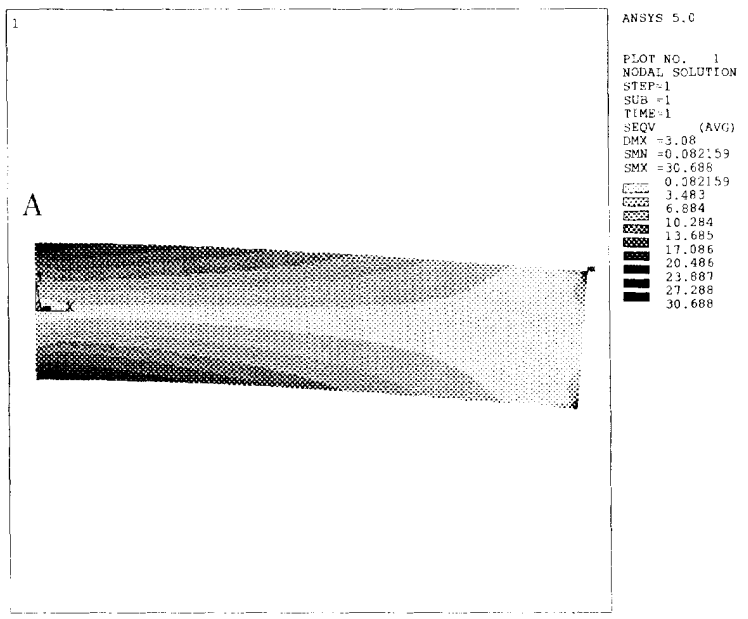


(a)

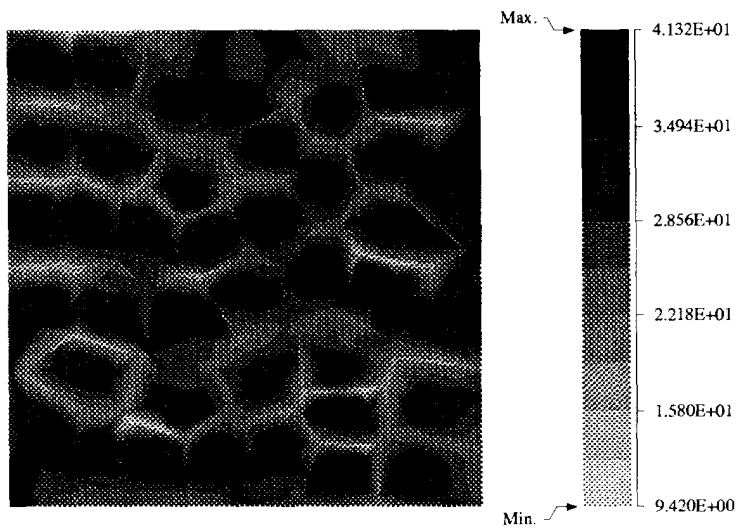


(b)

Fig. 15. Effective stress distribution for random orientation : (a) macroscopic stress ; (b) microscopic stress at point A.

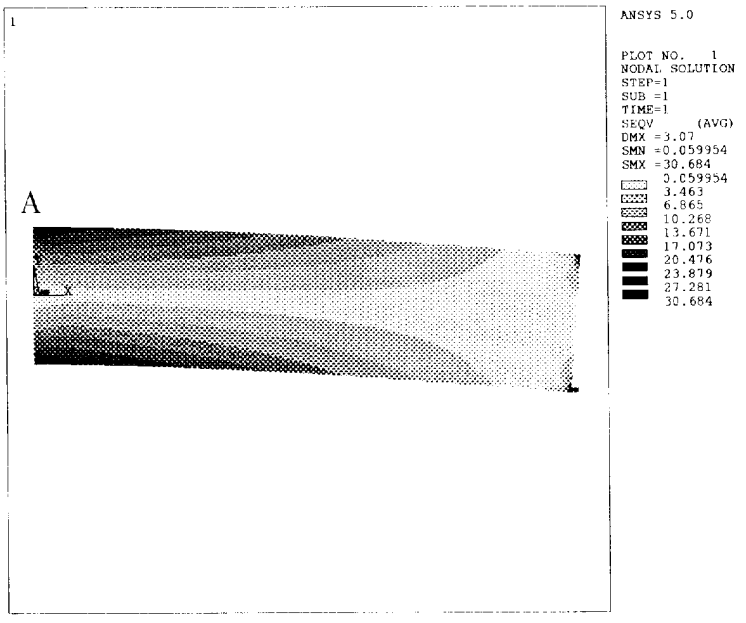


(a)

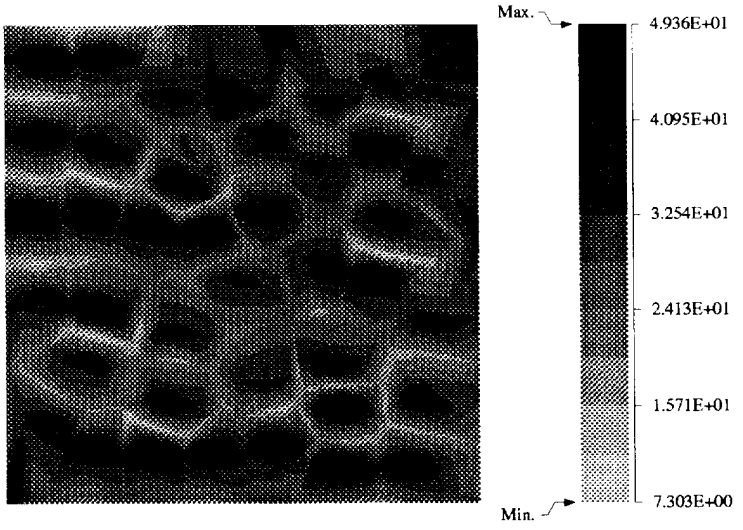


(b)

Fig. 16. Effective stress distribution for horizontal orientation: (a) macroscopic stress; (b) microscopic stress at point A.

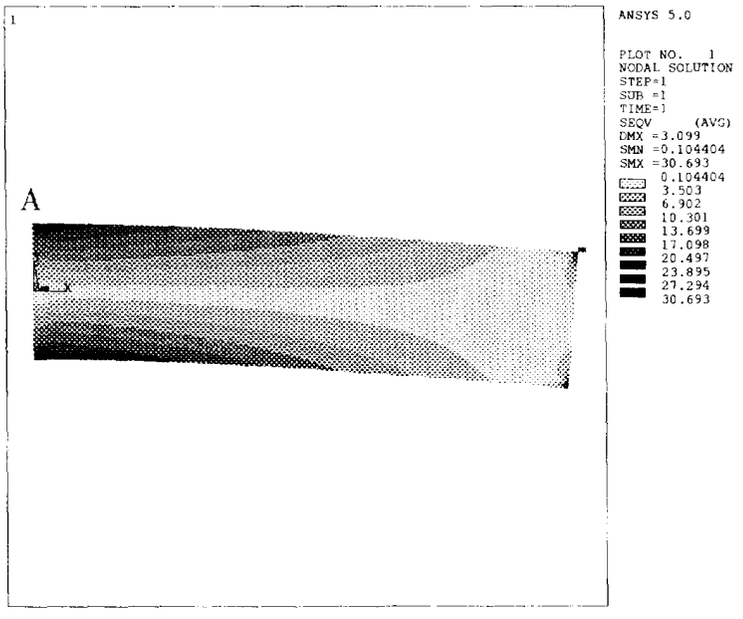


(a)

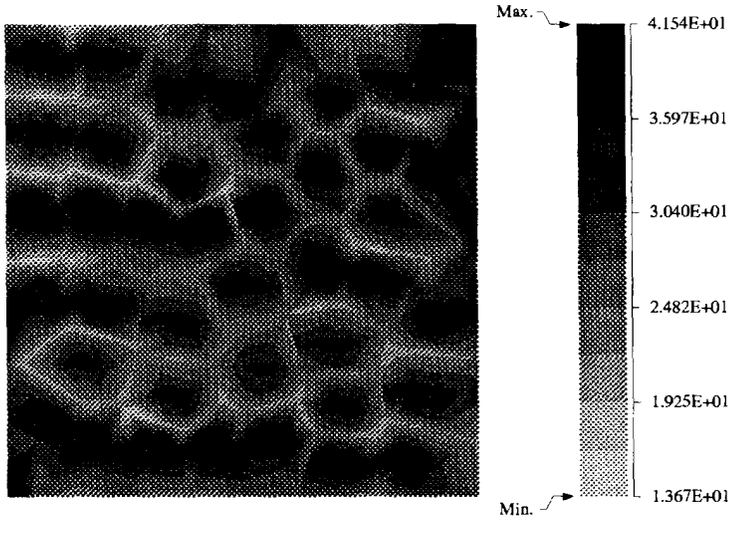


(b)

Fig. 17. Effective stress distribution for vertical orientation : (a) macroscopic stress ; (b) microscopic stress at point A.

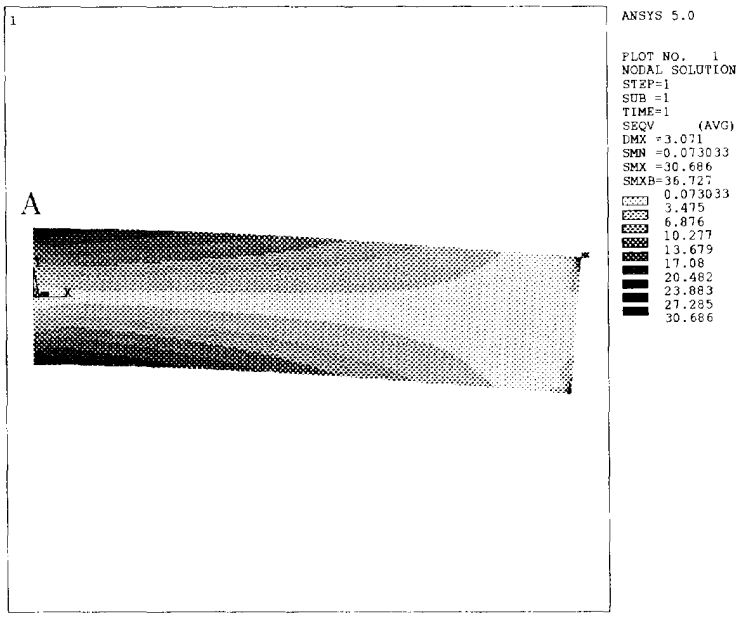


(a)

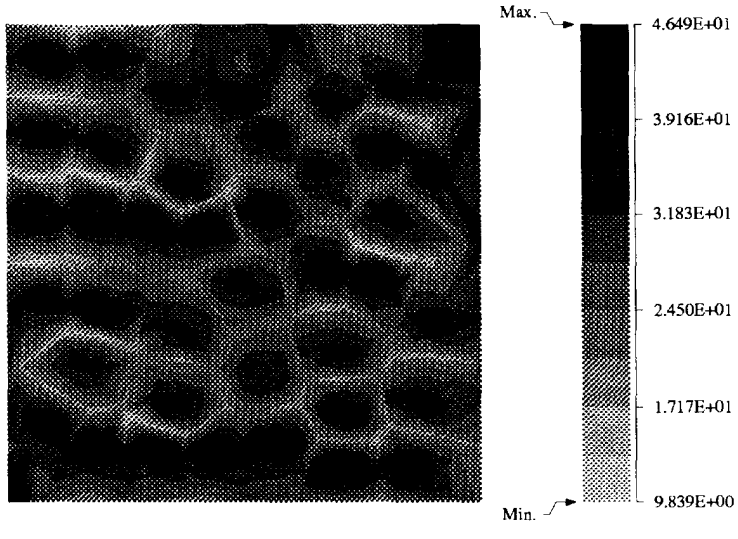


(b)

Fig. 18. Effective stress distribution for circular inclusion: (a) macroscopic stress; (b) microscopic stress at point A.

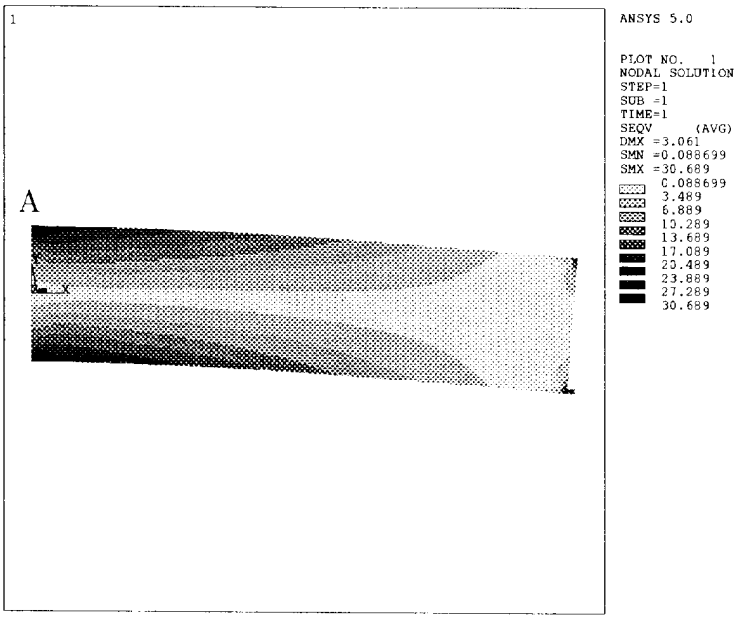


(a)

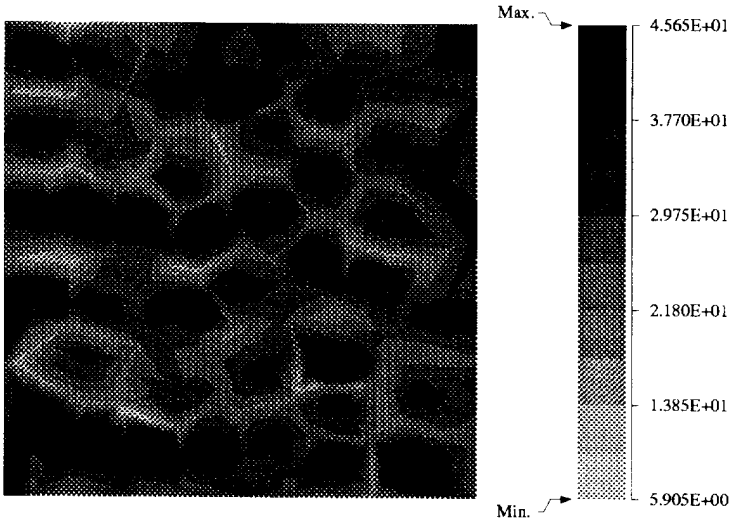


(b)

Fig. 19. Effective stress distribution for random size and shape : (a) macroscopic stress ; (b) microscopic stress at point A.

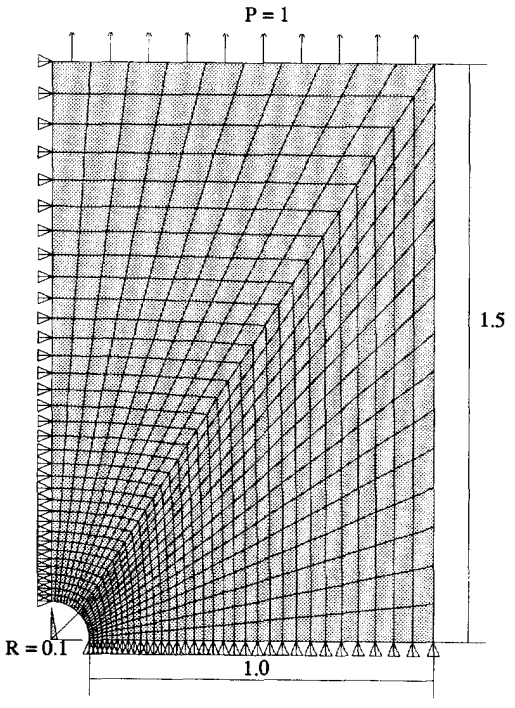


Fig. 6. Macroscopic FEM model for a plate with a hole.

a global point A, obtained by VCFEM. In the global structure, the homogenized macroscopic stress $\sigma_y$ has a maximum value at the point A. In the corresponding microstructure, the maximum micro-stress is 70% higher than this macroscopic stress. Microscopic stresses are higher in the fiber compared to the matrix material because of the higher value of Young's modulus. For the short fiber case, maximum $\sigma_y$ predicted by VCFEM is 5.5 GPa and that by HOMO2D is 5.75 GPa, which compare well with the results of Fish and Wagiman (1992) (5.75 by superposition and 5.6 with a strongly refined mesh). In Figs 9 and 10, the distribution of $\sigma_y$ along a horizontal section is plotted. The long fiber VCFEM results are in very good agreement with HOMO2D. Though the overall comparison is also good for the short fiber case, VCFEM results show stress jumps at the element boundaries due to the satisfaction of inter-element tractions in a total sense.

4.2. *Effect of microstructural morphology on homogenized coefficients and microscopic variables*

To study the effect of size, shape, orientation and location of second phase on the global–local behavior, five different material elements are analysed by the VCFEM. These base cells have the same second phase volume fraction but differ in size, shape and orientation. The microstructures shown in Fig. 11, can be classified as follows:

(i) elliptical inclusions with constant major and minor axes, having random orientation;
(ii) elliptical inclusions with constant major and minor axes, with horizontal major axes;
(iii) elliptical inclusions with constant major and minor axes, with vertical major axes;
(iv) circular inclusions with constant radius;
(v) inclusions of random shape and size, with random orientation.

The locations of the inclusions are arbitrary for all these microstructures. Constituent material properties are the same as in Example 1 of Section 4.1. Histograms, representing quantitative characterization of each microstructure, are shown in Figs 12 and 13. The inclusion to polygon area ratio is almost similar for cases (i)–(iv), except for case (v), for which the distribution has a wider range. Table 4 shows the homogenized material properties

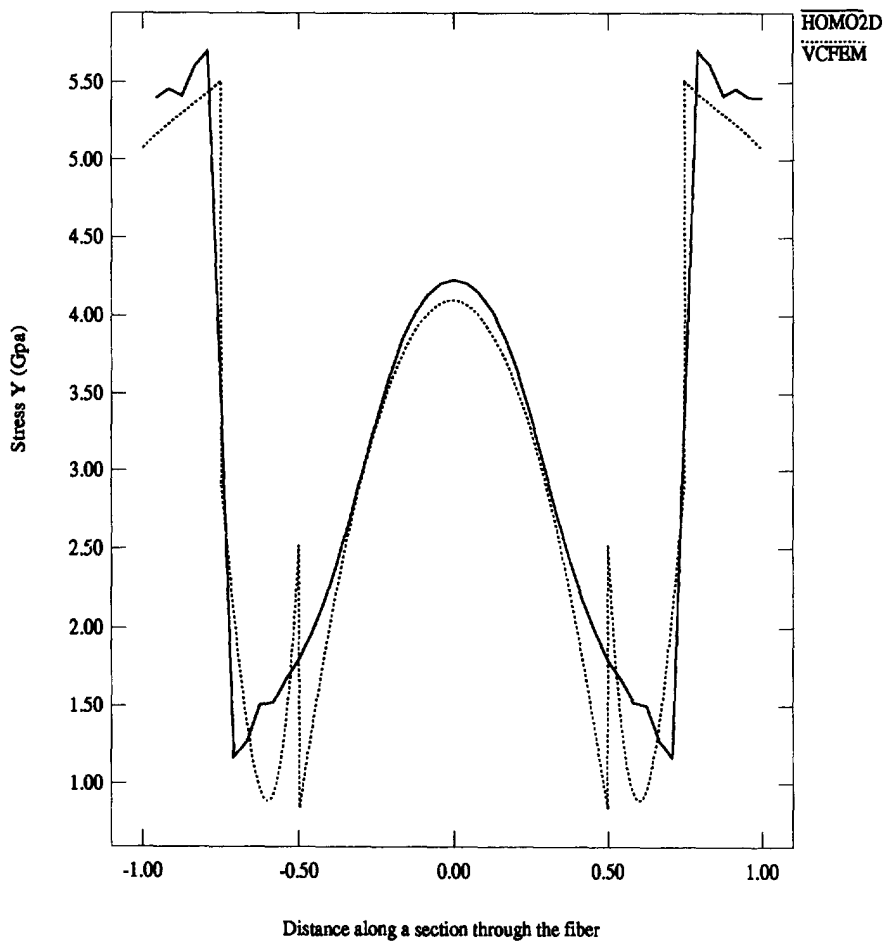


Fig. 9. Stress ($\sigma_{yy}$) distribution along the middle section of the short fiber base cell.

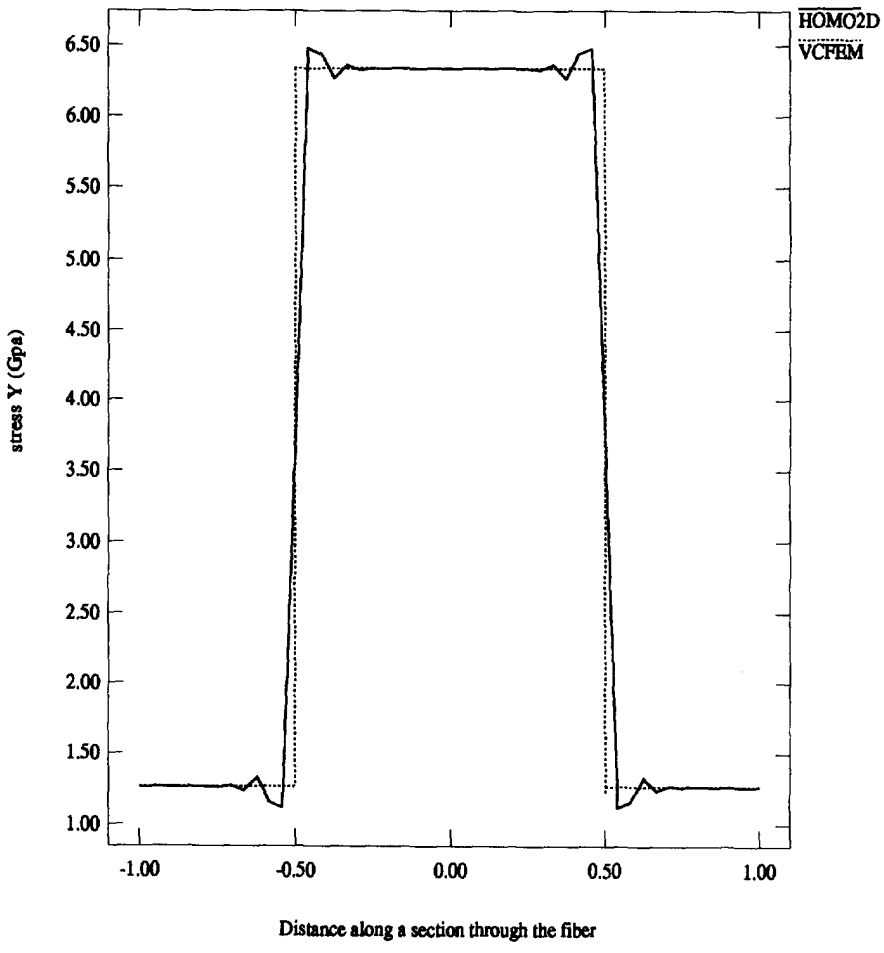


Fig. 10. Stress ($\sigma_y$) distribution along the middle section of the long fiber base cell.

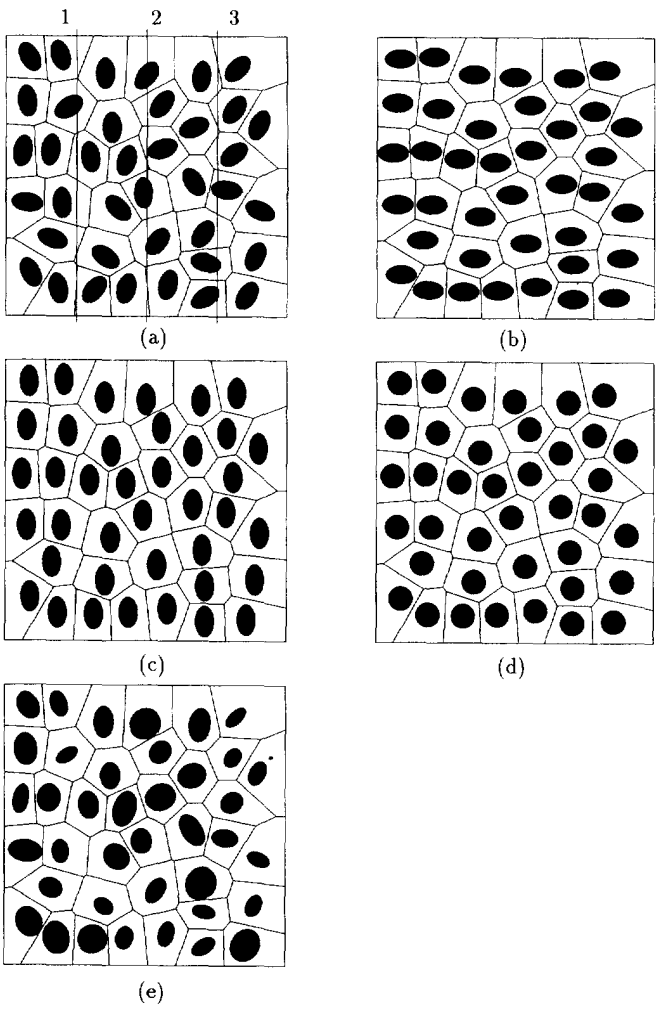


Fig. 11. Representative base cells for arbitrary dispersion with 20% second phase volume fraction: (a) random orientation; (b) horizontal orientation; (c) vertical orientation; (d) circular fiber; (e) random shape, size and orientation.

Table 3. Macroscopic stress values at point A

| | Short (VCFEM) | Short (HOMO2D) | Long (VCFEM) | Long (HOMO2D) |
|---|---|---|---|---|
| $\sigma_x$ (GPa) | 0.13314 | 0.13317 | 0.13191 | 0.13191 |
| $\sigma_y$ (GPa) | 3.1950 | 3.2874 | 3.7152 | 3.7152 |
| $\sigma_{xy}$ (GPa) | −0.06965 | −0.0700 | −0.07185 | −0.07185 |

for each microstructure computed by VCFEM. It is interesting to note that all the microstructures predict nearly identical values of material properties. Also, it can be seen that the homogenized behavior is nearly isotropic, which confirms experimentally observed phenomena for arbitrary dispersed microstructures. Case (iii) shows a slight difference between $E_1$ and $E_2$, indicating a stronger material response in the one-direction. Also, case (v) predicts little higher constants than case (i) because of the bigger size of the second phase.

For global analysis, a cantilever beam bending problem is solved with each of the homogenized material coefficients. Figure 14 shows the macroscopic FEM model. A point load of 1 GPa is applied at the free end. Though macroscopic stresses are similar for

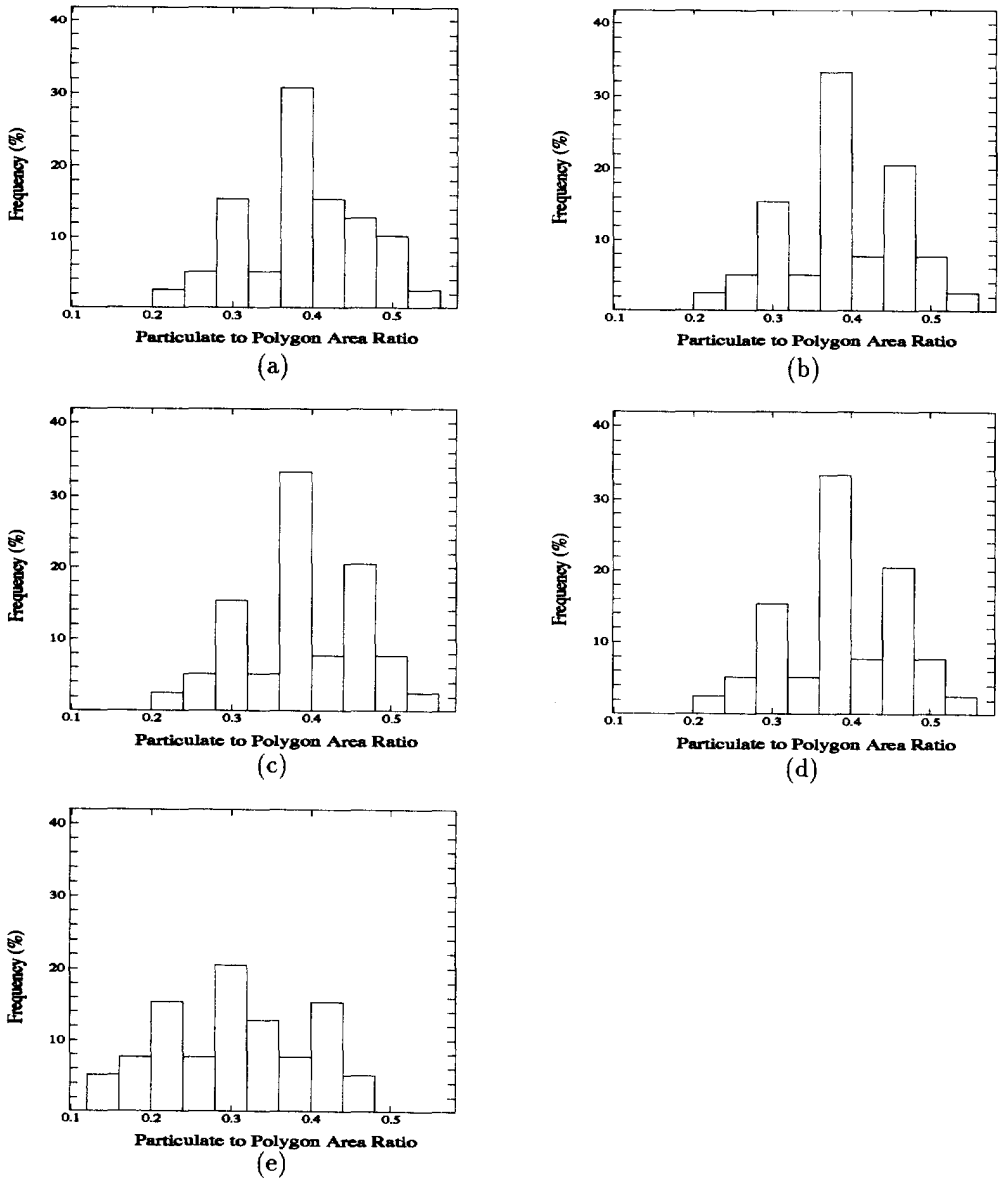


Fig. 12. Histograms of inclusion to neighboring polygon area ratio for different distributions: (a) random orientation; (b) horizontal orientation; (c) vertical orientation; (d) circular shape; (e) random shape and size.

Table 4. Homogenized material properties for different distribution of elliptic fiber

| Properties | E1 (GPa) | E2 (GPa) | G12 (GPa) | $\nu_{12}$ |
|---|---|---|---|---|
| Ellipse with random orientation | 89.22 | 89.70 | 33.38 | 0.3338 |
| Ellipse with horizontal orientation | 89.53 | 89.06 | 33.36 | 0.3277 |
| Ellipse with vertical orientation | 88.65 | 90.16 | 33.31 | 0.3234 |
| Circular | 89.47 | 89.46 | 33.40 | 0.3263 |
| Random shape and orientation | 89.78 | 90.16 | 33.53 | 0.3245 |

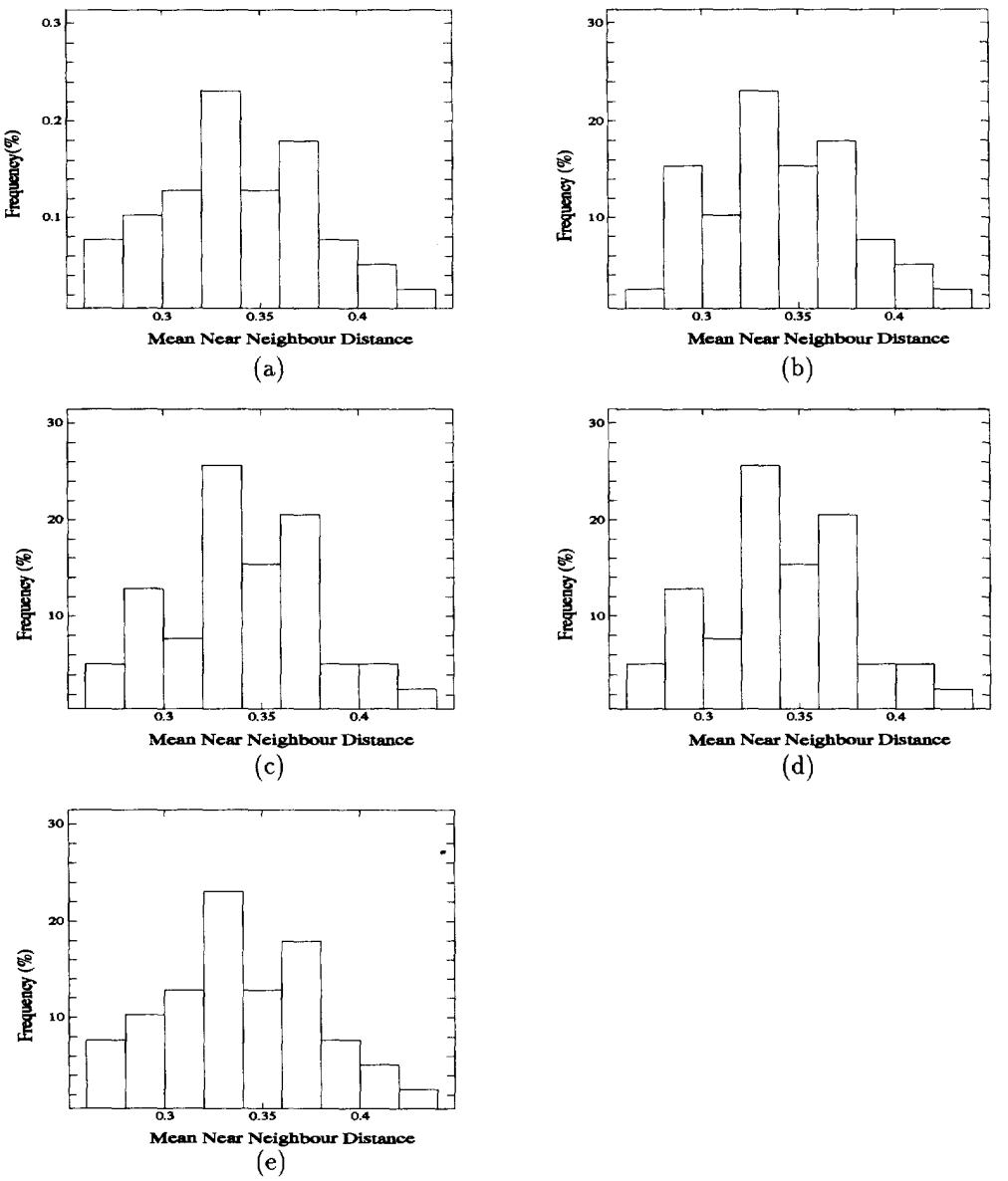


Fig. 13. Histograms of mean near neighbour distance for the different distribution: (a) random orientation; (b) horizontal orientation; (c) vertical orientation; (d) circular fiber; (e) random shape and size.

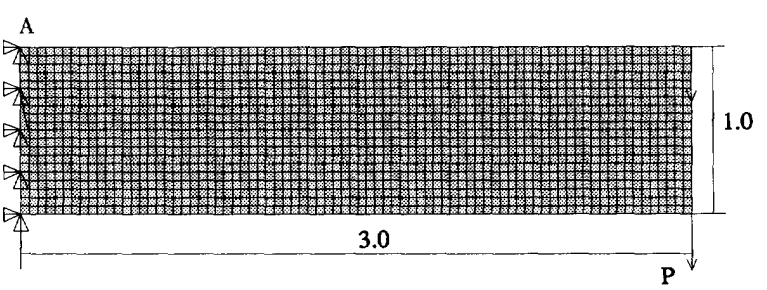


Fig. 14. FEM model for cantilever beam bending.

Table 5. Comparison of maximum microscopic and macroscopic stress for different distribution of elliptic fiber

| | Random | Horizontal | Vertical | Circle | Random shape |
|---|---|---|---|---|---|
| Micro-stress (GPa) | 41.32 | 49.36 | 41.54 | 46.49 | 45.65 |
| Macro-stress (GPa) | 30.688 | 30.684 | 30.693 | 30.686 | 30.683 |

all cases [(i)–(v)], because of near identical material properties, the microscopic stress distributions vary significantly with the morphology. Figures 15–19 show a comparison of effective macroscopic stress and microscopic stress distribution at point A. At this point (upper left corner) a maximum effective stress is expected. The maximum stresses in the microstructure are 30% to 60% higher than maximum homogenized stresses in the overall beam. The comparison is presented in Table 5. For this problem, the horizontally oriented microstructure experiences higher stress than the vertically orientated microstructure. This exhibits the possible design of microstructures for minimizing stresses. Figures 20–22 show plots for the effective stress along three sections in Fig. 11(a) for each microstructure.

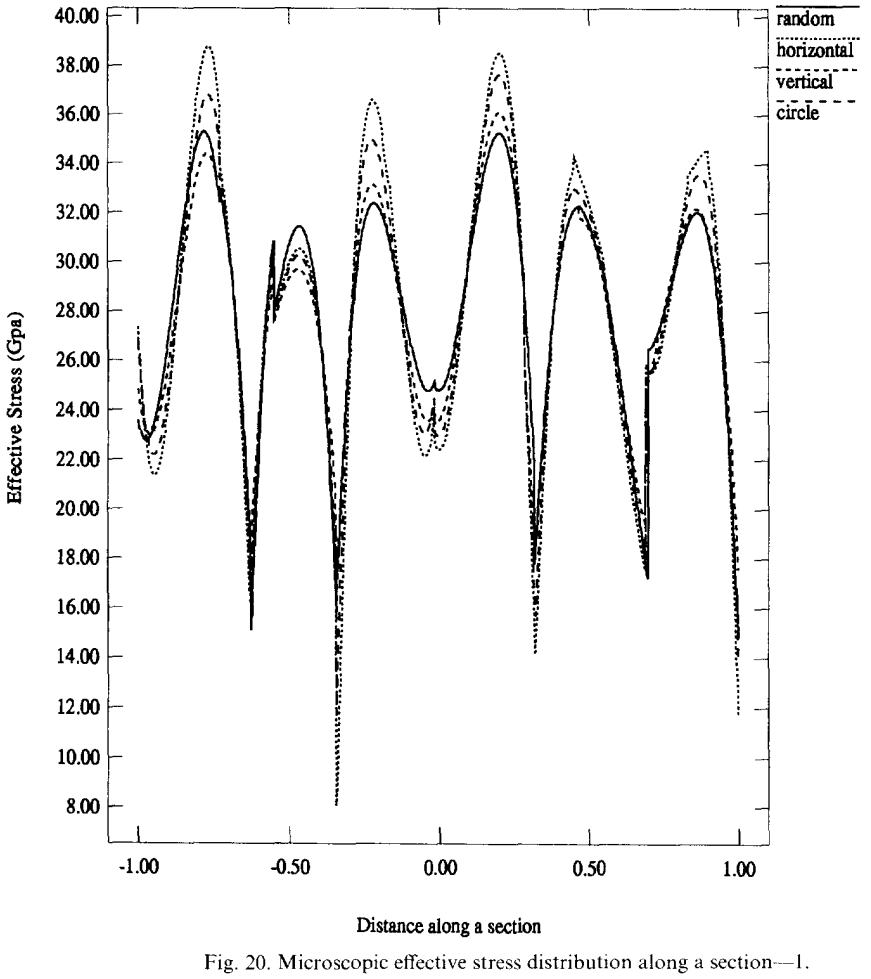


Fig. 20. Microscopic effective stress distribution along a section—1.

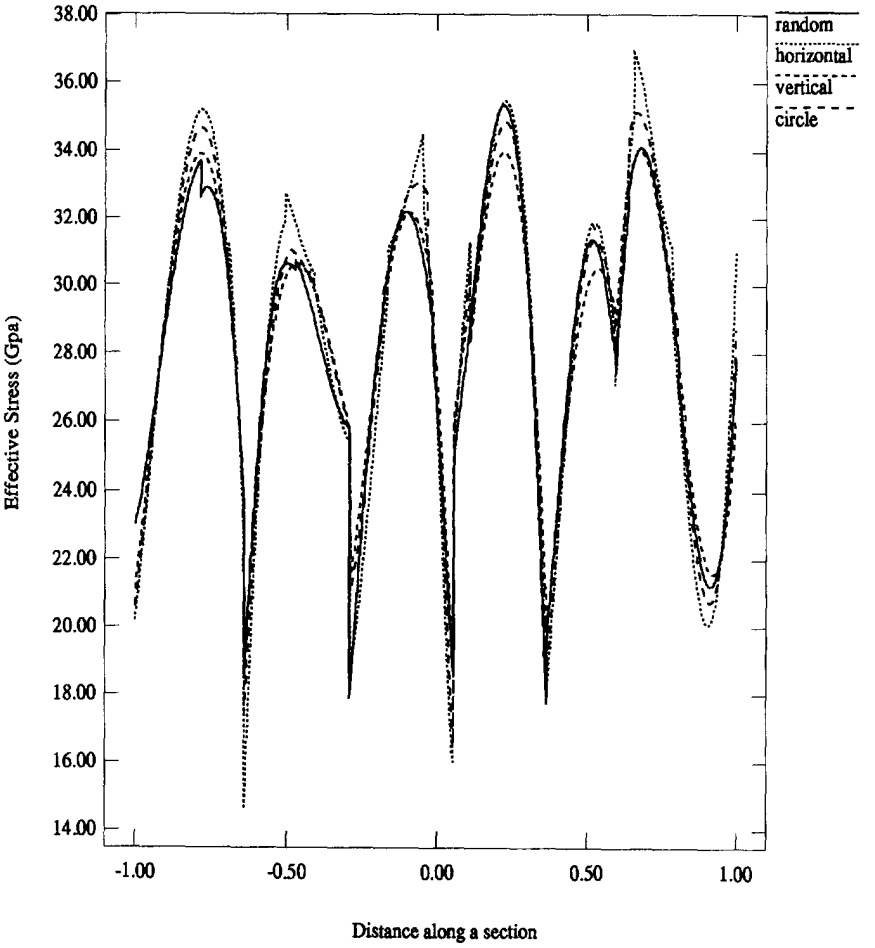


Fig. 21. Microscopic effective stress distribution along a section—2.

## 5. CONCLUSIONS

In this study, a microstructural Voronoi cell finite element method is coupled with the homogenization method for performing multiple scale analysis of heterogeneous structures with arbitrary microstructures. The microscopic Voronoi cell finite element model is created by Dirichlet tessellation of representative material elements or base cells. The coupled model projects a strong analysis tool for finding effective (homogenized) material properties as well as distributions of evolving macroscopic and microscopic variables. The stress based formulation of VCFEM makes the homogenization procedure simple and efficient.

Numerical examples conducted with the VCFEM conclusively prove the effectiveness of this method when compared with homogenization results of conventional finite element analyses, such as HOMO2D. Furthermore, it possesses tremendous advantages in discretizing complex microstructural models and results in a significantly reduced degree of freedom. Considering the large discrepancy in the number of elements, VCFEM shows very good accuracy. Though exact CPU time comparisons have not been made, it is generally observed that VCFEM is considerably more efficient. In conclusion, it may be inferred that the advantages in treating complex material morphologies with VCFEM makes it a very suitable candidate for analysing real materials. This is demonstrated in the experiments, where the random microstructure shows better agreement with experiments.

*Acknowledgements*——Support of this work by the U.S. Army Research Office through Grant No. DAAL03-91-G-0168 and by the National Science Foundation through Grant No. MSS-9301807 (Mechanics and Materials) is gratefully acknowledged. Computer support by a grant from the Ohio Supercomputer Center is also gratefully acknowledged.

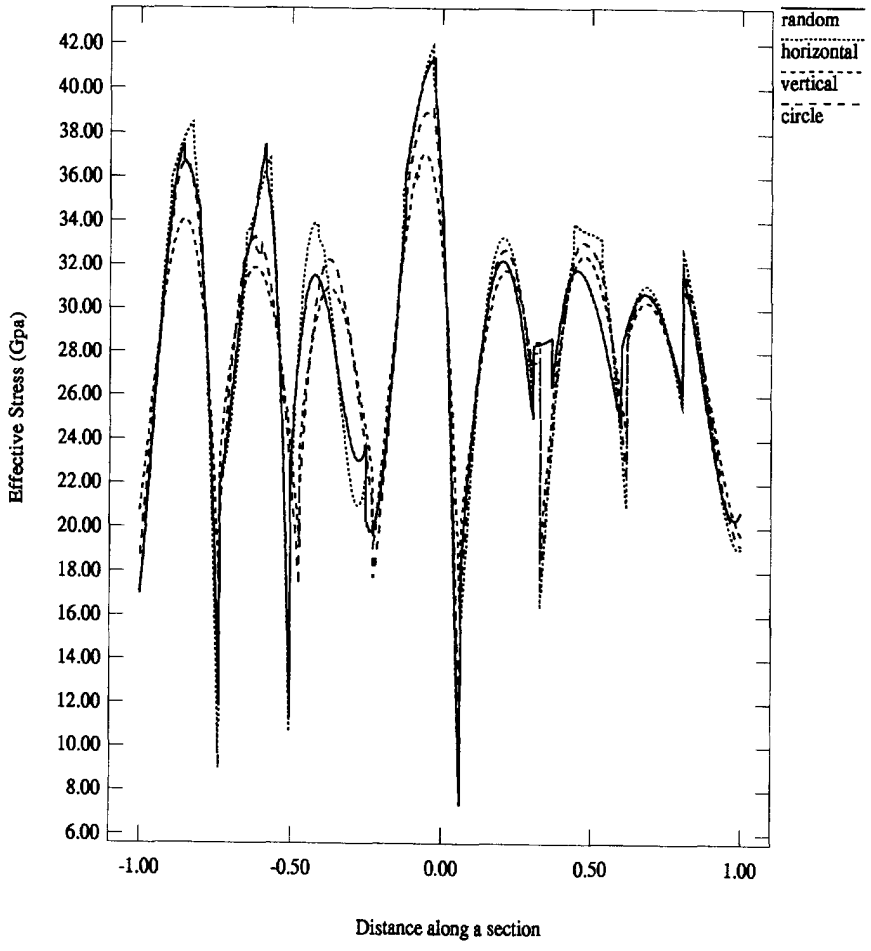


Fig. 22. Microscopic effective stress distribution along a section—3.

## REFERENCES

Bao, G., Hutchinson, J. W. and McMeeking, R. M. (1991). Plastic reinforcement of ductile matrices against plastic flow and creep. *Acta Metall. Mater.* **39.**

Benssousan, A., Lions, J. L. and Papanicoulau, G. (1978). *Asymptotic Analysis for Periodic Structures.* North Holland, Amsterdam.

Brockenbrough, J. R., Hunt, W. H. and Richmond, O. (1992). A reinforced material model using actual microstructural geometry. *Scripta Metall. Mater.* **27.**

Budiansky, B. (1965). On the elastic moduli of some heterogeneous materials. *J. Mech. Phys. Solids* **13,** 223–227.

Chen, H. S. and Acrivos, A. (1978). The effective elastic moduli of composite materials containing spherical inclusions at non-dilute concentrations. *Int. J. Solids Structures* **14,** 349–364.

Christensen, R. M. and Lo, K. H. (1979). Solutions for effective shear properties in three phase sphere and cylinder models. *J. Mech. Phys. Solids* **27,** 315–330.

Christman, T., Needleman, A. and Suresh, S. (1989). An experimental and numerical study of deformation in metal–ceramic composites. *Acta Metall. Mater.* **37,** 3029–3050.

Devries, F., Dumontet, H., Duvaut, G. and Lene, F. (1989). Homogenization and damage for composite structures. *Int. J. Numer. Meth. Engng* **27,** 285–298.

Eshelby, J. D. (1958). The determination of the elastic field of an ellipsoidal inclusion and related problems. *Proc. R. Soc. London* **241A,** 376–396.

Fish, J. and Wagiman, A. (1992). Multiscale finite element method for a periodic and nonperiodic heterogeneous medium. *Adaptive, Multilevel Hierarchical Comput. Strategies ASME-AMD* **157,** 95–117.

Fridy, J. M., Rouns, T. N., Lippert, K. B., Nes, E and Richmond, O. (1992). Characterization of 3-D particle distributions and effects on recrystallization studied by computer simulation. *Proc. 3rd Int. Conf. Aluminum Alloys* **2,** Trondheim, Norway.

Ghosh, S. and Liu, Y. (1994). Voronoi cell finite element method for micropolar thermoelastic heterogeneous materials (submitted).

Ghosh, S. and Mallett, R. L. (1994). Voronoi cell finite elements. *Computers Struct.* **50**(1), 33–46.

Ghosh, S. and Moorthy, S. (1994). Elastic–plastic analysis of heterogeneous microstructures using the Voronoi cell finite element method. Submitted to *Comp. Meth. Appl. Mech. Engng.*

Ghosh, S. and Mukhopadhyay, S. N. (1991). A two-dimensional automatic mesh generator for finite element analysis of randomly dispersed composites. *Computers Struct.* **41,** 245–256.

Ghosh, S and Mukhopadhyay, S. N. (1993). A material based finite element analysis of heterogeneous media involving Dirichlet tessellations. *Comp. Meth. Appl. Mech. Engng* **104,** 211–247.

Guedes, J. M. (1990). Nonlinear computational model for composite material using homogenization. Ph.D. Dissertation, University of Michigan, MI.

Guedes, J. M. and Kikuchi, N. (1991). Preprocessing and postprocessing for materials based on the homogenization method with adaptive finite element methods. *Comp. Meth. Appl. Mech. Engng* **83,** 143–198.

Hashin, Z. (1970). Theory of composite materials. In *Mechanics of Composite Materials* (Edited by F. W. Wend, H. Leibowitz and N. Perrone). Pergamon Press, Oxford.

Hashin, Z. and Strikman, S. (1963). A variational approach to the theory of the elastic behavior of multiphase materials. *J. Mech. Phys. Solids* **11,** 127–140.

Hill, R. (1965). A self consistent mechanics of composite materials. *J. Mech. Phys. Solids* **13,** 213–222.

Hori, M. and Nemat-Nasser, S. (1993). Double inclusion model and overall moduli of multiphase composites. *Mech. Mater.* **14,** 189–206.

Lynch, C. T. (1975). *CRC Handbook of Material Science*, Vol. II, p. 392. CRC Press, Cleveland.

Moorthy, S., Ghosh, S. and Liu, Y. (1994). Voronoi cell finite element model for thermo-elastoplastic deformation in random heterogeneous media. *Appl. Mech. Rev.* **47**(1), S207–S220.

Mura, T. (1987). *Micromechanics of Defects in Solids*. 2nd Edition. Kluwer Academic Publishers.

Nemat-Nasser, S., Yu, N. and Hori, M. (1993). Bounds and estimates of overall moduli of composites with periodic microstructure. *Mech. Mater.* **15,** 163–181.

Oleinik, O. A., Shamaev, A. S. and Yosifan, G. A. (1992). *Mathematical Problems in Elasticity and Homogenization.* North Holland, Amsterdam.

Pian, T. H. H. (1964). Derivation of element stiffness matrices by assumed stress distribution. *AIAA J.* **2,** 1333–1336.

Sanchez-Palencia, E. (1980). Non-homogeneous media and vibration theory. *Lecture Notes in Physics*, Vol. 127. Springer-Verlag, Berlin.

Spitzig, W. A., Kelly, J. F. and Richmond, O. (1985). Quantitative characterization of second phase populations. *Metallography* **18,** 235–261.

Toledano, A. and Murakami, H. (1987). A high order mixture model for periodic particulate composites. *Int. J. Solids Structures* **23,** 989–1002.

Tvergaard, V. (1990). Analysis of tensile properties for a whisker-reinforced metal matrix composite. *Acta Metall. Mater.* **38,** 185–194.